1 Title Page

Title: Comodulation reduces interindividual variability of circuit output

Abbreviated title: Reduction of circuit output variability

Author names and affiliations:

Anna C. Schneider, NJIT, 07102 Newark, NJ

Omar Itani, NJIT, 07102 Newark, NJ

Elizabeth Cronin, NJIT, 07102 Newark, NJ

Nelly Daur, NJIT, 07102 Newark, NJ

Dirk Bucher, NJIT, 07102 Newark, NJ

Farzan Nadim, NJIT, 07102 Newark, NJ

Corresponding author email address: farzan@njit.edu

Number of pages:

Number of figures: 10

Number of tables: 7

Number of words in abstract:

Number of words in introduction:

Number of words in discussion:

Conflict of interest: The authors declare no competing financial interests.

Acknowledgements:

Current affiliation of ACS: University of Kassel, 34132 Kassel, Germany

Funding by NIH MH060605 to FN and DB, DFG SCHN 1594/1-1 to ACS

2 Abstract

Ionic current levels of identified neurons vary substantially across individual animals. Yet, under similar conditions, neural circuit output remains remarkably similar, particularly in motor circuits. At any time, a neural circuit is influenced by multiple neuromodulators which provide flexibility to its output. These neuromodulators often overlap in their actions by modulating the same channel type or synapse yet have neuron-specific actions resulting from distinct receptor expression. With multiple neuromodulators, however, a common target is more uniformly activated across neurons. We propose that a baseline tonic (non-saturating) level of comodulation by convergent neuromodulators can reduce interindividual variability of circuit output. We tested this hypothesis in the pyloric circuit of the crab *Cancer borealis*. Multiple excitatory neuropeptides converge to activate the same voltage-gated inward current in this circuit, but different subsets of pyloric neurons have receptors for each peptide. We quantified the interindividual variability of the unmodulated pyloric circuit output by measuring the activity phases, cycle frequency and within-burst spike number and frequency. We then examined the variability in the presence of different combinations and concentrations of three excitatory neuropeptides. We found that at mid-level concentration (30 nM) but not at near-threshold (1 nM) or saturating (1 µM) concentrations, comodulation by multiple neuropeptides reduced the circuit output variability. Notably, the output variability of an isolated neuron was not reduced by comodulation at the mid-level concentration. Therefore, the reduction of circuit output variability is not due to a simple reduction of the variability of individual neuron excitability but emerges as a network effect.

3 Significance Statement

Behaviors as simple as reflexes or as complex as physiological responses to psychedelics can vary significantly among individuals, even when accounting for genotype and other variables. This behavioral variability results largely from variability of underlying neural circuits. Yet, in most cases, the CNS precisely controls behavior, and significant variability in CNS output may result in outputs deemed dysfunctional. We propose that additive actions of neuromodulators that target the same subcellular targets (comodulation) plays a central role in ensuring that neural circuits produce consistent circuit output in the face of extensive inter-individual variability.

4 Introduction

Historically, interindividual differences in animal behavior and the function of neural circuits that underlie these behaviors have been disregarded, and most studies have examined the average behavioral response and the mean activity of the neural circuits involved (Asahina et al. 2022). Yet, recent studies have shown that behaviors as simple as reflexes or as complex as physiological responses to psychedelics can vary significantly among individuals (Cerins et al. 2022; Moujaes et al. 2022; Xu et al. 2022), even when accounting for genotype and other variables (Hageter et al. 2021; Palavicino-Maggio and Sengupta 2022; Rihani and Sachse 2022). Behavioral variability results largely from variability of underlying neural circuits (Feierstein et al. 2015; Rihani and Sachse 2022; Tamvacakis et al. 2022) and such variability is present even in smaller invertebrate neural circuits (Goaillard et al. 2009; Goaillard and Marder 2021; Hamood and Marder 2014). Despite significant variability, a neural circuit can generate an output that is “good enough”(Nassim 2018) to produce a related behavior, such as in the asynchronous CNS control of fly flight (Boettiger and Furshpan 1952). Yet, in most cases, the CNS precisely controls behavior, and significant variability in CNS output results in outputs deemed dysfunctional. Thus, at some level, circuit output must become constrained enough to produce consistent and meaningful behavior.

Several factors have been proposed to promote a consistent output at the level of an individual neuron. These include correlations of ion channel expression (Golowasch et al. 2017; Khorkova and Golowasch 2007; Temporal et al. 2011; Tobin et al. 2009; Tran et al. 2019), output degeneracy (Goaillard and Marder 2021; Ransdell et al. 2013) and excitatory neuromodulation (Schneider et al. 2022). Whether any of these mechanisms result in reduction of interindividual variability at the circuit level remains mostly unexplored. Here, we propose that convergent comodulation could play an important role in ensuring that neural circuits produce consistent circuit output in the face of extensive interindividual variability (Grashow et al. 2009; Maloney 2021). Neuromodulation is conventionally considered to provide flexibility for neural circuit operation (Nadim and Bucher 2014). Yet, at any time, all neural circuits are comodulated by multiple substances (Harris-Warrick 2011; Marder 2012; Russo 2017). Some modulators control various aspects of excitability and synaptic output, and may target different neuron types (Harris-Warrick 2011). Others have limited but consistent actions across circuit neurons (Nadim and Bucher 2014). Consequently, different modulators often share subcellular targets, while remaining distinct in receptor levels or circuit neuron targets. Based on these facts, we propose an additional role for neuromodulation: that baseline (tonic) comodulation by multiple neuromodulators

that have convergent effects, but different neural targets or patterns of receptor expression, is essential for producing consistent circuit output.

We tested this hypothesis in the pyloric network of the stomatogastric ganglion (STG) of the crab *Cancer borealis*, which has been a long-standing testbed for neuromodulation (Daur et al. 2016; Marder et al. 2014). The pyloric circuit consists of identified neurons with known synaptic connections. Under physiological conditions it expresses regular periodic activity (~1 Hz) that can be easily quantified. Upon removal of all neuromodulatory inputs (decentralization) the pyloric rhythm is disrupted or significantly slowed and shows significant interindividual variability (Hamood et al. 2015). We measured several circuit activity attributes (cycle frequency, activity phases, etc.) after decentralization, and in the presence of one, two, or three neuropeptides, applied at the same total concentration. We then quantified the effect of comodulation on the interindividual variability of these attributes. We also used the same peptide combinations to assess the interindividual variability of the activity attributes of a single isolated pyloric neuron that is targeted by all three neuropeptides to see if comodulation of circuit variability is consistent with the effect of variability at the single-cell level. As a final step, we examined if a minimally constrained family of pyloric circuit model neurons captures the experimental observations on the effects of comodulation on interindividual variability.

5 Methods

5.1 Experimental preparation

Experiments were performed on the isolated stomatogastric nervous system (STNS) of male Jonah crabs (*Cancer borealis*) obtained from local fish markets and maintained in recirculating artificial seawater tanks at 12°C with 12:12 hour light-dark cycle until use. Crabs were anesthetized by chilling in ice for at least 30 min before removing the stomach. The STNS was carefully dissected from the stomach and pinned out in a Sylgard (Dow Corning) lined petri dish. All STNS preparations contained the the stomatogastric ganglion (STG), the anterior portion that contains modulatory projection neurons, and motor nerves including the lateral ventricular (lvn), pyloric dilator (pdn) and pyloric constrictor (pyn) nerves (Fig. 1A). The sheath around the STG was removed with fine tungsten pins to facilitate intracellular recording and the penetration of bath applied chemicals. A large petroleum jelly well was constructed around the STG, to allow for fast exchange of solutions, and constantly perfused with cold saline (11-12°C). Smaller wells for extracellular recordings were constructed around the lvn, pdn, and

110 pyn. To remove the influence of neuromodulatory projection neurons on the STG neurons, the
111 stomatogastric nerve (stn) was transected with fine scissors (decentralization).

112 5.2 Solutions

113 *C. borealis* saline contained (in mM): 440 NaCl, 26 $MgCl_2$, 13 $CaCl_2$, 11 KCl, 10 Tris base, 5 maleic acid,
114 buffered to pH 7.4. Proctolin (PROC; RS Synthesis), crustacean cardioactive peptide (CCAP; RS Synthesis),
115 and red pigment concentrating hormone (RPCH; GenScript) were prepared as 10^{-3} M aliquots (PROC and
116 CCAP in distilled water, RPCH in dimethyl sulfoxide: DMSO) and diluted to a final concentration in either
117 normal saline, or normal saline with picrotoxin (PTX), immediately before the experiments. The final
118 total modulator concentrations were 10^{-9} M (low), $3x10^{-8}$ M (mid), and 10^{-6} M (high). In a few initial
119 experiments, a concentration of 10^{-8} M was used as mid. The total modulator concentration (low, mid,
120 or high) was held constant in comodulator applications so that with two modulators each was 1/2 of the
121 total concentration and with three modulators each was 1/3 of the total concentration.
122 For experiments that assessed single neuron excitability, synapses were blocked with picrotoxin (PTX;
123 Sigma-Aldrich). PTX was dissolved 10^{-2} M in DMSO (Fisher Scientific) and stored as stock solution at 4°C.
124 Immediately before the experiment, PTX stock solution was diluted to a final concentration of 10^{-5} M in
125 saline.

126 5.3 Electrophysiology

127 Thin stainless steel pin electrodes were inserted in petroleum jelly wells around the lvn, pdn, and pyn
128 to record the pyloric rhythm extracellularly. The extracellular electrodes were connected to a
129 differential AC amplifier (Model 1700, A-M Systems). We recorded the pyloric rhythm in the intact STNS,
130 20 min after decentralization, and 10 min after washing in each of the sequence of neuropeptides
131 applied at different concentrations and combinations in the following order. In total, we obtained three
132 different datasets, each with intact and decentralized conditions in addition to: 1) low proctolin (P), low
133 proctolin + CCAP (PC), low proctolin + CCAP + RPCH (PCR), mid P, mid PC, mid PCR, wash out; 2) high P;
134 3) high PC. Because modulators were added sequentially, we did not wash out with saline between
135 modulatory conditions. To minimize the variability that can be caused by changing environmental or
136 experimental factors we typically did these experiments simultaneously with two preparations in the
137 same dish and at the same time of the day.
138 To examine the variability of intracellular properties, we first identified the lateral pyloric (LP) and the
139 two pyloric dilator (PD) neurons in an intact preparation by matching the intracellular activity to the

extracellular activity on the lvn and pdn, and by their characteristic intracellular voltage waveforms. We then decentralized the preparation, impaled the LP neuron with two electrodes and both PD neurons with one electrode each and washed in PTX for at least 15 minutes until inhibitory postsynaptic potentials in the PD neuron (from the presynaptic LP neuron) disappeared and LP inhibition during PD bursts was greatly reduced. We then ran current clamp protocols as described in (Schneider et al. 2022) in the LP neuron while hyperpolarizing the PD neurons by -5 nA to eliminate the remaining PTX-insensitive PD to LP synaptic inhibition. Each set of protocols was repeated in decentralized, mid P, mid PC, mid PCR, and wash. For *f-I* curves, we incrementally depolarized LP in 0.5 nA steps from 0 to 5 nA. To measure *f-I* hysteresis, we inverted the protocol, going from 5 nA back to 0 nA. We ran each protocol twice and used the average of both sweeps for analysis (see below). To measure rebound properties, we used two differently scaled protocols. First, we hyperpolarized LP five times with -5 nA for 10 s with an interval of 10 s in between. This interval was long enough for LP to return to initial conditions before the next sweep (Schneider et al. 2022). In addition, we hyperpolarized LP periodically with twenty 1 s-on/1 s-off, -5 nA current pulses, which is in the physiological range of LP inhibition by the PD neurons. To analyze the response to the periodic hyperpolarization, we only used the last 10 pulses to avoid the transient response of the LP neuron to the first few pulses (Schneider et al. 2022).

Intracellular signals were amplified with Axoclamp 900A amplifiers (Molecular Devices). All recordings were digitized at 5 kHz (Digidata 1440A, Molecular Devices) and recorded with Clampex 10.6 (Molecular Devices).

5.4 Data analysis

All data were imported from Clampex to Matlab (version 2021a) with abfload (Hentschke 2011), and analyzed with custom written scripts and the CircStat toolbox (Berens 2009). Statistical tests were performed with SigmaPlot (version 12.0, Systat Software) with a significance level of $\alpha = 0.05$. We used ANOVA with Tukey's post-hoc test if the data passed tests for normal distribution (Shapiro-Wilk) and equal variance (Levene). If one of these tests failed, we used ANOVA on ranks with Dunn's post-hoc test to compare metrics between different modulatory conditions.

Pyloric rhythm attributes

To quantify the pyloric rhythm, we measured from the extracellular recordings the cycle period (time from the beginning of one PD burst to the next) and cycle frequency (reciprocal of PD cycle period), and, for PD, LP, and PY each, the phases of burst onset and termination (the respective latency divided by cycle period) relative to PD onset, number of spikes per burst, and spike frequency within a burst. Note

171 that in each animal PD exists in two copies and PY in 3-5 copies. Since we obtained the number of spikes
172 and spike frequency from extracellular recordings, the number of spikes and spike frequencies we
173 reported was for all active PD or PY units, respectively detected on pdn or pyn. Abbreviations of all
174 pyloric rhythm attributes are given in Figure 1.

175 A complete quantification of the pyloric circuit activity requires the existence of a triphasic rhythm. In
176 our data summaries we indicate the number of preparations of each dataset that were analyzed. The
177 missing preparations did not express rhythmic activity.

178 We used different metrics to measure the interindividual variability of the different attributes. For
179 F_{cycle}, *#spks*, and F_{spks} we used the adjusted coefficient of variation (CV), which is the standard deviation
180 divided by the mean and adjusted for sample size (Haldane 1955). Since CV only is meaningful for data
181 on a ratio scale, we used the angular variance as a measure of variability for phase data. Briefly, each
182 phase value is represented as a vector composed of the sine and cosine of its angle on a unit circle with
183 a length of 1. Averaging these vectors gives a resultant (r-) vector with the mean phase as direction and
184 a length (r) between 0 and 1 that depends on the spread of the data. If all phase data were similar, and
185 therefore located at the same point on the unit circle, the r-vector would have a length of 1. If all data
186 were evenly spread around the circle, r-vector length would be 0. Angular variance is, by definition, 1 –
187 r. Since the circuit neurons do not have independent activity phases, we computed the correlation
188 coefficient matrices for all phases for each modulatory condition and their eigenvalues. We then
189 summed the eigenvalues, which gave us a measure for the variability of all phase data.

190 Single neuron excitability attributes

191 We analyzed the intracellularly recorded data as described in (Schneider et al. 2022). In brief, we fit
192 the *f-I* curves with the power function

$$f(I) = a(I - I_0)^b, f \geq 0 \qquad \text{Eq. 1}$$

193 where a is a scaling factor approximating the maximum spike frequency, I_0 is the (calculated) current
194 level that first elicited spikes, and the power b (set to $0 \leq b \leq 1$ to limit the *f-I* curve to a sublinear
195 function) measures the nonlinearity of the *f-I* curve. Hysteresis was calculated as the ratio of the average
196 spike frequency for injected current between 2 to 4 nA with increasing current injection divided by the
197 average spike frequency between 2 to 4 nA with decreasing current injection.

198 For the rebound protocols, we considered all five sweeps for the 10 s current injection and only the
199 last 10 sweeps for the 1 s current injection. We measured the average latency between the end of the
200 current injection and the first spike. We fitted the cumulative spike histogram with the sigmoid

$$f(t) = \frac{a}{1 + \exp\frac{t - t_{1/2}}{k}} \qquad \text{Eq. 2}$$

where a is the total number of spikes in the interval between current injections, $t_{1/2}$ is the sigmoid midpoint time relative to the end of current injection, and k is the slope factor.

As metric for interindividual variability, we used either the adjusted CV, or standard deviation for interval measures (for which CV was not applicable), of the fit parameters, hysteresis, and latency.

5.5 Modeling

Models of the pyloric circuit

Computational models based on the pyloric circuit were constructed with the circuit diagram given in Fig. 1, but with only one PD and 2 PY neurons. Models were constructed and run using the Python (ver. 3.7) (Van Rossum and Drake 2009) interface to NEURON (ver. 8.2.1) (Carnevale and Hines 2006). Pyloric neurons other than AB were modeled to have two compartments: an S/N compartment representing the soma, neurites and dendrites, and an A compartment representing the axon. The AB neuron was represented by a single somatic compartment, based on our previous model of the pacemaker group (Daur et al. 2019). Synaptic connections were modeled to follow sigmoidal transfer functions with activation and decay time constants depending on the presynaptic membrane potential. All model parameters are described in Table 1.

Table 1: Main components of the pyloric circuit model. Model equations are provided in the supplement Figure 10-1. The parameters for intrinsic currents and synapses are, respectively, in the supplements Figure 10-2 and Figure 10-3.

Cells	Synapses	Intrinsic currents
AB	AB → LP, PY1, PY2 (inhibitory)	leak
PD	PD → LP, PY1, PY2 (inhibitory)	Na, CaS, MI
LP	LP → PD, PY1, PY2 (inhibitory)	KS, A, Kd
PY1	PY1, PY2 → LP (inhibitory)	
PY2	AB ↔ PD (symmetric electrical coupling)	
	LP ↔ PY1, PY2 (rectifying electrical coupling)	

Initial family of models

To build an initial family of pyloric circuit models, we started with a general form of the model as described above. We then allowed the maximal conductances of intrinsic currents and synapses to vary. We used the simulation-based inference python toolbox (SBI v0.20.0) to select 175 models that complied with attributes of activity within the following selection criteria:

- Cycle Frequency > 0,
- Phases: PD off < 1; LP on < 1; LP off < 0.65; PY on < 1; PY off < 1.2,
- Spike numbers: PD > 2; LP > 2; PY (1 & 2 combined) > 1.

To simulate decentralization (Hamood et al. 2015), we ran simulations of each model while scaling down the value of g_{MI} of all neuron types multiplicatively until the model pacemakers (AB and PD) ceased to produce bursting oscillations. We chose the values of g_{MI} at the cusp of pacemaker activity as our decentralized case to allow for quantifiable rhythms.

Modeling peptide comodulation

We modeled peptide modulation by increasing the maximal g_{MI} values multiplicatively across each cell type. To capture multiple axes of peptide modulation, we scaled g_{MI} along three axes: pacemakers (AB/PD), LP, and PYs, resulting in a 3D grid spanning multiplicative scalars from 1 to 1.75 in increments of 1/16. Across the 175 models, we measured interindividual variability of each attribute at each point in the grid using circular variance (for phases) or CV (all other attributes) and reported it as percent change with respect to the variability of the decentralized case.

6 Results

6.1 Comodulation at mid concentrations reduced interindividual variability of the circuit activity attributes.

The intact stomatogastric nervous system consists of the stomatogastric ganglion (STG), which includes the pyloric circuit neurons, as well as the esophageal ganglion (OG) and the paired commissural ganglia (CoGs; Fig. 1A). The STG neurons receive input as hormones and neurotransmitters released from the axons of the OG and CoG neurons that project through the stomatogastric nerve (stn) and many of which are spontaneously active at any time. These projection neurons co-release a variety of small-molecule and peptide neurotransmitters that modulate the pyloric circuit and enable its spontaneous rhythmic activity. We characterized the pyloric rhythm by determining output pattern

249 attributes from simultaneous extracellular recordings of the three motor nerves, lvn, pdn and pyn (Fig.
250 1A). The core circuit that generates the pyloric rhythm (Fig. 1B) includes the anterior burster (AB)
251 interneuron as well as two pyloric dilator (PD), lateral pyloric (LP) and 3-5 pyloric constrictor (PY) motor
252 neurons. The axons of the three motor neuron types, PD, LP and PY, project bilaterally through the lvn
253 and their action potentials can be readily separated by simultaneous extracellular recordings of lvn, pdn
254 and pyn that show the well-characterized triphasic pyloric burst sequence of these neurons (Fig.
255 1C)(Marder and Bucher 2007).

256 We measured pyloric output pattern attributes (marked in Fig. 1C) across different modulatory
257 states, with intact descending input, after decentralization (see below), and after application of
258 neuropeptides (Fig. 2A). With intact descending inputs, spontaneous activity of projection neurons
259 ensures that the pyloric neurons are always bathed in a soup of modulatory neurotransmitters,
260 including several peptides that are co-released by these projection neurons (Nusbaum et al. 2017). In
261 vitro, all modulatory inputs can be removed by blocking or severing the projection nerve (stn), a
262 procedure we refer to as decentralization (Fig. 2A). Removing all neuromodulatory input to the STG by
263 decentralization greatly slows down or even disrupt the pyloric rhythm (Hamood and Marder 2015).
264 Bath application of excitatory neuropeptides can restore a peptide-specific version of the pyloric rhythm
265 (Marder and Thirumalai 2002; Marder and Weimann 1992; Swensen and Marder 2001). We used three
266 excitatory neuropeptides that target distinct but overlapping neurons in the pyloric circuit (Fig. 2A), but
267 all converge on the same target ion channel within these subsets. This target is a voltage-gated inward
268 current referred to as I_{MI} (Golowasch and Marder 1992; Schneider et al. 2021; Swensen and Marder
269 2000). Proctolin activates I_{MI} in AB, PD, LP, and most PY neurons, while both CCAP and RPCH activate I_{MI}
270 only in AB and LP neurons (Fig. 2A) (Swensen and Marder 2001). Additionally, both PROC and CCAP
271 enhance synaptic currents in the reciprocal connections between the pacemaker neurons and LP (Li et
272 al. 2018), but effects on the pacemaker to PY and PY to LP synapses have not been studied. RPCH
273 increases the strength of the LP to pacemaker synapse (Atamturktur and Nadim 2011; Thirumalai et al.
274 2006), but its effect on other synapses has not been studied.

275 Our goal was to test whether comodulation by multiple excitatory neuropeptides reduces
276 interindividual variability of circuit output. To examine this hypothesis, we bath applied combinations of
277 one (PROC: P), two (PROC + CCAP: PC), and three (PROC + CCAP + RPCH: PCR) neuropeptides at the same
278 total low and mid concentrations (Fig. 2B&C) in several preparations and examined the variability of
279 multiple circuit output attributes (see Materials and Methods for detailed description). Statistical results

for all pyloric circuit attributes of this dataset are listed in Table 2. Raw data are provided in Figure 2-1 and Figure 3-1.

Decentralization decreased cycle frequency compared to intact preparations. While application of one or more neuropeptides at low or mid concentrations to the decentralized preparation tended to increase cycle frequency, it was only with application of three modulators at mid concentration that cycle frequency recovered to values statistically similar to those in the intact condition (Fig. 2D, upper panel). Upon decentralization, the cycle frequency coefficient of variation (CV) approximately doubled compared to the intact state and remained high when we applied one, two, or three neuropeptides at low concentration (Fig. 2D, lower panel). However, when we applied increasing numbers of peptides at mid concentration, the CV consistently decreased toward its intact value. Washing out the modulators increased CV as expected.

A similar effect was observed for the on and off phases of all three neurons, PD, LP, and PY (Fig. 3). The burst onset (on) and end (off) phases of individual pyloric neurons within each cycle is a major determinant of the proper function of this central pattern generator, and these activity phases remain surprisingly consistent across individual animals despite large variations in cycle frequency (Anwar et al. 2022; Bucher et al. 2005; Goaillard et al. 2009). Decentralization and application of neuropeptides affected the mean phases of PD and LP, but not of PY (Fig. 3A top panels). However, there was a large effect on the inter-animal variability of the phase values. We measured variability of activity phases as the circular variance (1 - r; Fig. 3A top left inset; also see Methods). Circular variance of all phases greatly increased upon decentralization and was somewhat reduced by application of neuropeptides (Fig. 3A bottom panels). Notably, for all phases, circular variance consistently decreased when we increased the number of applied neuropeptides at mid concentration but not at low concentration (Fig. 3A bottom panels).

Because of recurrent connectivity of the pyloric circuit (Fig. 1A), the PD, LP and PY on and off phases are not independent of each other. To account for the covariation of the phases, we computed the covariance matrix of all five phases in each modulatory condition. Total variation can be measured as the trace (equivalently, sum of the eigenvalues) of this matrix (Fig. 3B). The resulting pattern of total variation of phase under the different modulatory conditions was the same as for cycle frequency and for individual phases: Variability increased with decentralization but consistently decreased when we increased the number of neuropeptides at mid concentrations. No consistent pattern was seen at low concentrations (green bars).

311 We also quantified two other important output attributes of the pyloric circuit neurons, the number
312 of spikes per burst and the intra-burst spike frequency. In PD, the mean number of spikes was largely
313 unaffected by decentralization and modulator application (Fig. 4A top left). In contrast, decentralization
314 decreased the PD mean spike frequency, and only mid concentrations peptide application returned this
315 attribute toward its intact values (Fig. 4B top left). LP generated significantly more spikes per burst in PC
316 and PCR at mid concentrations (Fig. 4A top middle). This was also reflected in the LP mean inter-burst
317 spike frequency (Fig. 4B top middle). In contrast, mean spiking activity of PY remained unchanged across
318 all conditions.
319 The changes in interindividual variability of the spiking activity (measured as CVs) were somewhat
320 different from the consistent changes we saw for the cycle frequency and activity phases. First, the CVs
321 of PD number of spikes and spike frequency did not consistently decrease with adding modulators at
322 mid concentration but rather was similar across those conditions. However, in LP and PY variability still
323 decreased with additional modulators at mid concentration (purple bars in Fig. 4A, B bottom left).
324 Second, the CVs of the LP number of spikes and spike frequency was in fact largest in the intact
325 condition. Yet, for both the LP and PY neurons, the CVs of both spiking attributes were reduced by
326 adding modulators at mid concentration (purple bars in Fig. 4A, B bottom middle & right).
327 One caveat of these experiments was that, because we had applied the neuropeptide sequentially at
328 low and then mid concentrations (see, e.g., Fig. 2C), the preparations recorded with mid concentration
329 of P, PC and PCR had all been pre-exposed to low concentrations of all three modulators (low PCR). To
330 ensure that the reduction of interindividual variability with comodulation at mid concentration is not
331 due to a history-dependent effect, we repeated these experiments by applying P, PC and PCR at only
332 mid concentration levels. These experiments effectively replicated the same results that most attributes
333 of the pyloric circuit output showed a reduction of variability with increased numbers of peptide
334 comodulators (Fig. 5, Table 3; raw data are provided in Figure 4-1). Once again, the CVs of PD spike
335 attributes did not reduce with comodulation. In these experiments, we also did not see a consistent
336 reduction in variability of PY spike attributes or end phase.
337

Table 2: ANOVA results for pyloric rhythm parameters at low and mid modulator concentrations. If tests for normality or equal variance failed, results are for ANOVA on ranks. Groups are intact, decentralized, P [low], PC [low], PCR [low], P [mid], PC [mid], PCR [mid], wash. p values smaller than α are printed in bold. N: number of animals; df: degrees of freedom; res: residual. Note that, despite the significant effect from ANOVA, the pairwise comparison for PY on phase did not show any significant differences between groups (Fig. 3A).

N	parameter	normality	variance	test statistic	df	res.	p
15	Cycle frq	fail		H = 36.645	8		**<0.001**
15	PD off	fail		H = 24.794	8		**0.005**
15	LP on	fail		H = 19.799	8		**0.011**
15	LP off	fail		H = 37.006	8		**<0.001**
15	PY on	fail		H = 20.498	8		**0.009**
15	PY off	fail		H = 15.495	8		0.050
15	PD spikes	pass	pass	F = 3.365	8	119	**0.002**
15	PD spike frq	fail		H = 29.773	8		**<0.001**
14	LP spikes	pass	pass	F = 21.217	8	111	**<0.001**
14	LP spike frq	pass	fail	H = 50.238	8		**<0.001**
15	PY spikes	fail		H = 9.413	8		0.309
15	PY spike frq	fail		H = 9.958	8		0.268

Table 3: ANOVA results for pyloric rhythm attributes mid modulator concentrations (different dataset than in Table 2). If tests for normality or equal variance failed, results are for ANOVA on ranks. Groups are intact, decentralized, P [mid], PC [mid], PCR [mid], wash. p values smaller than α are printed in bold. N: number of animals; df: degrees of freedom; res: residual.

N	attribute	normality	variance	test statistic	df	res.	p
25	Cycle frq	fail		H = 61.109	5		**<0.001**
25	PD off	fail		H = 33.152	5		**<0.001**
25	LP on	pass	fail	H = 37.630	5		**<0.001**
25	LP off	pass	fail	H = 61.122	5		**<0.001**
25	PY on	pass	pass	F = 7.677	5	134	**<0.001**
25	PY off	pass	pass	F = 7.224	5	134	**<0.001**
25	PD spikes	fail		H = 31.084	5		**<0.001**
25	PD spike frq	fail		H = 5.576	5		0.350
25	LP spikes	pass	fail	H = 94.633	5		**<0.001**

25	LP spike frq	pass	pass	F = 29.448	5	131	**<0.001**
25	PY spikes	fail		H = 41.5592	5		**<0.001**
25	PY spike frq	pass	pass	F = 3.009	5	134	**0.013**

6.2 Compared to single peptide modulators, comodulation at mid concentrations did not reduce interindividual variability at the single-neuron level.

In a previous study we showed that neuropeptide modulation at saturating concentration reduces the interindividual variability of excitability attributes of the synaptically isolated LP neuron (Schneider et al. 2022). This finding raises the possibility that the reduction of circuit output variability arising by increasing numbers of comodulatory peptides at mid-level concentration may be a consequence of a similar reduction at the level of individual pyloric neurons. To examine this hypothesis, we measured single-neuron interindividual variability using the same protocols as in Schneider et al. (2022), but with increasing numbers of comodulators applied at mid concentration. We focused on the synaptically isolated LP neuron because it exists only in a single copy in each animal, and it is targeted by all three neuropeptides that we used in this study (Swensen and Marder 2001).

The first excitability attribute that we examined was the spike frequency vs. input current relationship (*f-I* curve). We measured the *f-I* curves by applying increasing and decreasing current steps and measured the firing frequency at each step (Fig. 6A). In order to compare these data across individuals, we parameterized the *f-I* curves across the range of applied currents by fitting these data with a sublinear power function $f(I) = a(I - I_0)^b$ where I_0 is the zero-intercept, a is the slope and the power b is between 0 and 1, ensuring the curve is at most linear (Fig. 6B fit curve; also see Methods). Both the slope factor a, and the exponent b, but not I_0, were different in mean value in the presence of neuropeptides compared to the unmodulated condition, indicating that a higher LP spike rate in the presence of the neuropeptides (ANOVA results in Table 4; raw data are provided in Figure 6-1). In general, fit parameter variability was lower when one or more peptide modulators were present, but there was no consistent reduction in variability with the addition of comodulators (Fig. 6C).

As seen in the voltage trace of Figure 6A, the *f-I* curve shows hysteresis, in that the firing frequency for each current step depends on whether it is measured on the increasing or decreasing leg of injected currents (Fig. 6B). We quantified hysteresis, as detailed in the Methods, by calculating the ratio between the mean *f* value on the increasing and decreasing legs of injected currents within the shaded region (2 – 4 nA) of Fig. 6B. Thus, a value greater than 1 means that LP was spiking at a higher frequency the current

375 changed in increasing direction. Even though neuropeptides influenced hysteresis, they did not change
376 its variability (Fig. 6C).
377
378 *Table 4: ANOVA (on ranks) results for f-I parameters. Groups are decentralized, P [mid], PC [mid], PCR [mid], wash. p values*
379 *smaller than α are printed in bold. N: number of animals; df: degrees of freedom.*

N	parameter	normality	test statistic	df	p
17	a	fail	H = 24.667	4	**<0.001**
17	b	fail	H = 29.801	4	**<0.001**
17	I_0	fail	H = 3.680	4	0.451
19	hysteresis	fail	H = 27.796	4	**<0.001**

380
381 LP is a follower neuron and, during normal pyloric activity, generates burst of spikes upon rebound
382 from inhibition. To examine the post-inhibitory rebound properties of LP, we hyperpolarized the isolated
383 LP neuron for 10 s and characterized the spiking activity in the 10 s window after release from inhibition
384 in different modulatory conditions (Fig. 7A). We did so by measuring the latency from the end of
385 inhibition to the first spike, and also characterizing the properties of the spike histogram in the 10 s
386 window following the inhibition (Fig. 7B). We characterized the spike histogram by fitting a sigmoid
387 function to the cumulative spike count (Fig. 7C).
388 Adding one or several neuropeptides at mid concentration significantly changed the mean values of
389 the fit parameters of the sigmoid but not the rebound latency (Fig. 7D top row; ANOVA results in Table
390 5; raw data are provided in Figure 7-1). All fit parameters increased with neuropeptides compared to the
391 decentralized control condition, indicating that LP was overall firing more spikes in longer bursts,
392 consistent with the increased excitability seen in the *f-I* curves. Neuropeptides increased the likelihood
393 of LP rebound from inhibition and overall decreased the variability of the rebound parameters
394 compared to the two unmodulated conditions (decentralized and wash). However, we observed a
395 decrease of variability with increasing numbers of neuropeptides only for the fit parameters $t_{1/2}$ and k,
396 but not for the latency or the total number of spikes within a rebound burst (Fig. 7D bottom row). The
397 decrease of variability was present even when the parameters were not statistically different between
398 the modulatory conditions.
399

400 *Table 5: ANOVA results for 10 s rebound parameters. If tests for normality or equal variance failed, results are for ANOVA on*
401 *ranks. Groups are decentralized, P [mid], PC [mid], PCR [mid], wash. p values smaller than α are printed in bold. N: number of*
402 *animals; df: degrees of freedom; res: residual.*

N	parameter	normality	variance	test statistic	df	res.	p
19	latency	fail		H = 3.385	4		0.495
19	a	pass	pass	F = 8.665	4	77	**<0.001**
19	$t_{1/2}$	fail		H = 28.343	4		**<0.001**
19	k	fail		H = 13.148	4		0.011

403

404 In the intact pyloric circuit, LP is periodically inhibited by a group of pacemaker neurons and typical
405 pyloric cycle frequencies range from 0.5 to 2 Hz. Therefore, we modified the rebound protocol
406 hyperpolarization to 1 s on / 1 s off and 20 repeats (Fig. 6A). As shown previously (Goaillard et al. 2010;
407 Schneider et al. 2022), LP rebound only reaches steady state after several cycles (Fig. 6B). Therefore, we
408 only included the last 10 sweeps in our analysis and examined the same rebound parameters as for the
409 10 s rebound protocol (Fig. 6C). In contrast, the application of neuromodulators at mid concentration
410 did not significantly change any of the parameters with this faster protocol (Fig. 6D, ANOVA results in
411 Table 6; raw data are provided in Figure 8-1). Even though the kinetics of the modulator-activated
412 current I_{MI} are fast, the lack of modulatory effects indicate that the levels of I_{MI} itself or potential
413 dynamic interactions with calcium-dependent currents (Schneider et al. 2021) are not sufficient to
414 change the parameter values at normal pyloric cycle frequencies. Furthermore, while the metrics of
415 variability do not increase with the addition of comodulators, the reduction of variability across animals
416 is minor and does not recover after washing (Fig. 6D).

417

418 *Table 6: ANOVA results for 1 s rebound parameters. If tests for normality or equal variance failed, results are for ANOVA on*
419 *ranks. Groups are decentralized, P [mid], PC [mid], PCR [mid], wash. p values smaller than α are printed in bold. N: number of*
420 *animals; df: degrees of freedom; res: residual.*

N	parameter	normality	variance	test statistic	df	res.	p
19	latency	fail		H = 5.329	4		0.249
19	a	pass	pass	F = 2.371	4	76	0.060
19	$t_{1/2}$	pass	pass	F = 0.765	4	76	0.551
19	k	fail		H = 4.068	4		0.397

421

422 ## 6.3 Peptide comodulation at saturating concentrations did not reduce variability of
423 circuit activity attributes below that with a single peptide.

424 So far, we have shown in this study that increasing the number of comodulatory neuropeptides at
425 mid concentrations, but not at low concentrations, decreased the variability of several pyloric circuit
426 rhythm attributes across animals. In contrast, at the single neuron level, additional mid-concentration
427 comodulatory reduction of variability is absent or ambiguous even though peptide modulation does
428 reduce variability. This latter finding is consistent with our previous findings that peptide modulation at
429 saturating concentrations (at or above 1 µM) reduces single-neuron variability but addition of a second
430 comodulatory peptide (i.e., 1 µM each) does not further reduce it (Schneider et al. 2022). However, at
431 saturating concentrations, convergent modulators may also occlude one another's actions. This raised
432 the question of whether comodulation reduction in variability of the full circuit output attributes.

433 We addressed this question with the same two modulators used in the Schneider et al (2022) study.
434 Figure 9 summarizes the results of applying P and PC at a total concentration of 1 µM to the
435 decentralized preparation (ANOVA results in Table 7; raw data are provided in Figure 9-1). In contrast to
436 the experiments at low and mid concentrations, we only used experiments where the pyloric rhythm
437 continued when the preparation was decentralized. In these experiments, cycle frequency was
438 significantly higher in the intact condition (Fig. 9A), and decentralization impacted the off phases of PD
439 and LP and the on phase of PY (Fig. 9B). For frequency and phases, variability across individuals was
440 lower with modulators than without (Fig. 9A-B). Additionally, the variability at high concentrations was
441 even lower than in three modulators at mid concentration (indicated by the hollow purple bars in Fig.
442 9A-C bottom row). This was also the case for the sum of the eigenvalues of the phase covariance matrix
443 (Fig. 9C). At saturating concentrations, the variability across animals was in the same range as in the
444 intact condition. But even though the overall variability of frequency and phase was lower at high
445 concentrations, the addition of a comodulator did not further reduce variability in a consistent manner
446 as it did at mid concentrations. Variability metrics for spike number (Fig. 9D) and spike frequency
447 (Fig. 9E) within a burst, however, decreased with the addition of a comodulator but the variability in
448 high modulator concentrations was comparable to that in mid concentrations. Taken together, these
449 results show that comodulation at saturating concentrations is not as consistently reducing variability at
450 the network level as comodulation below saturating concentrations.
451

Table 7: ANOVA results for pyloric rhythm attributes at high modulator concentrations. If tests for normality or equal variance failed, results are for ANOVA on ranks. Groups are intact, decentralized, P [high], PC [high], wash. p values smaller than α are printed in bold. N: number of animals; df: degrees of freedom; res: residual.

N	attribute	normality	variance	test statistic	df	res.	p
20	Cycle frq	pass	pass	F = 43.965	3	54	**<0.001**
20	PD off	pass	pass	F = 9.373	3	54	**<0.001**
20	LP on	pass	fail	H = 1.457	3		0.692
20	LP off	pass	fail	H = 30.555	3		**<0.001**
20	PY on	pass	pass	F = 14.001	3	54	**<0.001**
20	PY off	fail		H = 2.913	3		0.405
20	PD spikes	fail		H = 4.285	3		0.232
20	PD spike frq	fail		H = 13.449	3		**0.004**
20	LP spikes	pass	pass	F = 28.269	3	54	**<0.001**
20	LP spike frq	pass	pass	F = 30.227	3	54	**<0.001**

6.4 Should excitatory comodulation generically reduce variability?

As mentioned above, excitatory modulatory peptides influence the pyloric circuit by activating the voltage-gated inward current, I_{MI}, and by increasing synaptic efficacy. Because these peptide modulators have distinct but overlapping targets, the effect of additive comodulation would be to primarily activate I_{MI} in additional pyloric neurons and perhaps modulate more synapses. Increasing the levels of I_{MI} in a neuron would increase its excitability. Is it possible then that simply targeting more pyloric neurons with higher and higher levels of I_{MI} would generically (i.e., without additional constraints) result in a reduction of interindividual variability? We examined this possibility using computational modeling.

That the basic triphasic pyloric pattern can be generated in models with widely varying levels of ion current maximal conductances has been well established (Prinz et al. 2004). We therefore started with a family of 175 pyloric model circuits, each with the same neuron types and connectivity (Fig. 1B), expressing the same cohort of ionic currents (Fig. 10AB), but with a distinct combination of maximal conductance values (see Methods for a detailed description; equations and parameters in Figure 10-1, 10-2, and 10-3). We modeled peptide neuromodulation by increasing the maximal g_{MI} levels in each target neuron (Fig. 10B). We ensured that each model circuit expressed a triphasic motor pattern similar to that observed in the biological circuit (Fig. 10C). Variability of circuit output attributes was measured

472 as the circular variance (for phases, as in the biological experiments) or CV (for all other attributes)
473 across the 175 model circuits, under different levels of modulatory input.
474 To characterize the effects of comodulation, we assumed first that each modulator targets only one
475 of three groups of neurons. We did so by splitting the circuit neurons into three groups: the pacemaker
476 (AB and PD) neurons, the LP neuron and the PY neurons. We started with the family of model circuits in
477 the unmodulated state and then increased g_{MI} independently in each of the three groups. For each
478 group, g_{MI} was increased from its baseline unmodulated value, in multiplicative steps, across the whole
479 family of model circuits. Because g_{MI} was increased independently in each of the three groups, we
480 obtained a 3D grid representation of our modulatory space (Fig. 10C). Note that the effect of any
481 neuromodulator that targets more than one group by activating different levels of I_{MI} in different neuron
482 groups would also be represented in this grid.
483 We analyzed the effect of neuromodulators on variability for each attribute by plotting how
484 variability is reduced or increased across the 3D grid explained above (Fig. 10D-E). The variability of cycle
485 frequency was reduced by increasing g_{MI} in the pacemakers (as seen in the increase in the blue color
486 along the horizontal axis of each box of the top row in Figure 10D). Increasing g_{MI} in LP, however,
487 increased the variability of cycle frequency, but only when g_{MI} values were low in PY (as seen in the
488 increase in the black color along the vertical axis of the leftmost 4 boxes of the top row in Figure 10D).
489 The variability of LP spike number and spike frequency was insensitive to g_{MI} in the pacemakers, reduced
490 with g_{MI} in LP and increased with g_{MI} in PY. The variability of PY spike number and frequency decreased
491 with g_{MI} in the pacemakers but was mostly insensitive to g_{MI} in LP or even in the PYs themselves. This is
492 probably because PY spiking variability was most sensitive to the variability of cycle frequency.
493 The variability of the burst onset (φ_{on}) and end (φ_{off}) phases showed a remarkably different pattern
494 than that of cycle frequency or neuronal spiking activities (Fig. 10E). Surprisingly, φPD_{off} (i.e., the PD duty
495 cycle) became more variable with increased g_{MI} in the pacemakers. Its variability also increased with g_{MI}
496 in LP but was reduced by g_{MI} in PY. φLP_{on} became less variable with g_{MI} in LP and to a smaller extent with
497 g_{MI} in PY, but increased in variability with g_{MI} in the pacemakers, probably because it is closely tied to
498 φPD_{off}. In contrast, φLP_{off} variability increased with g_{MI} in the pacemakers, but this was compensated for
499 by g_{MI} in PY which greatly reduced this variability. Somewhat surprisingly, φLP_{off} variability was
500 insensitive to g_{MI} in LP. φPY_{on} became more variable with g_{MI} in either the pacemakers or LP, but this
501 was compensated for by g_{MI} in PY itself when the pacemaker g_{MI} was not too strong. In our models,
502 φPY_{off} was very close to 1 (the onset of the next cycle) and did not show much variability.

To understand how increasing g_{MI} leads to reduction of variability, we examined how the distribution of the values of an output attribute may change as a function of g_{MI}. We show three examples of this effect in Figure 10F. Increasing g_{MI} in the pacemakers shifts the distribution (shown as normalized probability density function) of cycle frequency to larger values, but across the family of models, cycle frequency remains below an upper bound of ~2 Hz (Fig. 10F top panels). Thus, the rising segment of the density function curve is shifted to the right much more than its falling segment, resulting in a narrower density function and therefore a lower CV. A similar narrowing of the density function is seen for LP spike frequency, when g_{MI} is simultaneously increased in the pacemakers and LP (Fig. 10F middle panels). For the activity phases, reduction of variability could also result from shifting the density function to the left. For example, increasing g_{MI} in PY can result in restricting the maximum value of φLP_{off} without changing its minimum (Fig. 10F bottom panels). This occurs because the end of the LP burst is in great part due to the inhibition it receives from the PY neurons (see Fig. 10C) and strengthening the PY burst (earlier burst onset and more spikes per burst) by increasing g_{MI} would constrain the end of the LP burst.

To see how comodulation of the model circuits resulted in an overall reduction of variability of circuit activity, we plotted the overlapping regions in which variability of individual output attributes was reduced (Fig. 10G). We did this separately for activity phases (circular variances, shown in red) and all other attributes (CVs, shown in blue). The resulting graph provides two sets of information. First, it shows that as levels of g_{MI} increase across all three neuron groups, akin to increased comodulation, there is reduction of variability of all CVs but only up to a certain g_{MI} level, akin to an intermediate concentration (increase in blue regions from bottom left to top right in each panel and from left to right across panels). Second, it shows that although increasing g_{MI} in all three neuron groups could also reduce the circular variance of all phase attributes (red), the range of g_{MI} for which this overall reduction occurs has little overlap with the region in which CVs of other attributes are reduced (overlap shown in magenta). From this information we conclude that the reduction of variability across both phase and other attributes that we observed in the biological circuit does not arise generically with our simplifying assumptions used to model the circuit and its modulation.

7 Discussion

In summary, the interindividual variability of almost all pyloric rhythm attributes was reduced by increasing the number of comodulatory neuropeptides at mid concentration but not at low concentration. The low concentration of 10^{-9} M is close to threshold of I_{MI} activation for proctolin and

CCAP (Li et al. 2018). Since we were keeping the total modulator concentration constant, the inconsistent changes in variability at low concentrations could be due to threshold effects. Furthermore, reduction in variability can happen even if modulator application is not changing the mean value of an attribute.

Using comodulation to reduce variability still allows for flexibility of the output, e.g., by upregulation of a specific neuropeptide that shifts the output towards a peptide-specific pattern.

- low concentrations: Threshold effects increased variability
- high concentrations:
    - Saturation of neuropeptide targets. Target variability is high across animals and the failure to reduce variability with increasing numbers of neuropeptides could be a consequence of the target variability.
    - However, overall variability was lower at [high] than at [mid], indicating that higher, but non-saturating, concentrations could be more effective in reducing variability at increased numbers.

At the network level increasing the number of neuropeptides reduced animal-to-animal variability of most attributes only at mid concentrations.

Each modulator targets a subset of cells, but in each neuron multiple neuropeptides can converge on the same target.

Increasing the numbers of neuropeptides activates all subsets and reduces interindividual variability by averaging out the specific effects of any individual neuropeptide.

This is a network effect since the mere increase in excitability of a single neuron by comodulation does not reduce its variability (these results for [mid] and the other variability paper for [high]).

Modeling suggests that the interplay of neurons with individually increased excitability can reduce the network output variability.

8 References

Anwar H, **Martinez D**, **Bucher D**, **Nadim F**. Inter-Animal Variability in Activity Phase Is Constrained by Synaptic Dynamics in an Oscillatory Network. *eNeuro* 9, 2022.

Asahina K, **de Bivort BL**, **Grunwald Kadow IC**, **Yapici N**. Editorial: Revisiting Behavioral Variability: What It Reveals About Neural Circuit Structure and Function [Online]. *Frontiers in Behavioral Neuroscience* 16, 2022https://www.frontiersin.org/articles/10.3389/fnbeh.2022.956388 [3 May 2023].

Atamturktur S, **Nadim F**. Effects of neuromodulator RPCH on short-term dynamics of a key synapse in an oscillatory network of crab Cancer borealis. *Journal of Applied Biological Sciences* 5: 59–72, 2011.

566 **Berens P**. CircStat: A MATLAB Toolbox for Circular Statistics. *Journal of Statistical Software* 31: 1–21,
567 2009.

568 **Boettiger EG**, **Furshpan E**. The mechanics of flight movements in diptera. *The Biological Bulletin* 102:
569 200–211, 1952.

570 **Bucher D**, **Prinz AA**, **Marder E**. Animal-to-animal variability in motor pattern production in adults and
571 during growth. *J Neurosci* 25: 1611–9, 2005.

572 **Carnevale NT**, **Hines ML**. The NEURON Book. Cambridge University Press.

573 **Cerins A**, **Corp D**, **Opie G**, **Do M**, **Speranza B**, **He J**, **Barhoun P**, **Fuelscher I**, **Enticott P**, **Hyde C**.
574 Assessment of cortical inhibition depends on inter individual differences in the excitatory neural
575 populations activated by transcranial magnetic stimulation. *Sci Rep* 12: 9923, 2022.

576 **Daur N**, **Nadim F**, **Bucher D**. The complexity of small circuits: the stomatogastric nervous system.
577 *Current Opinion in Neurobiology* 41: 1–7, 2016.

578 **Daur N**, **Zhang Y**, **Nadim F**, **Bucher D**. Mutual Suppression of Proximal and Distal Axonal Spike
579 Initiation Determines the Output Patterns of a Motor Neuron [Online]. *Frontiers in Cellular Neuroscience*
580 13, 2019https://www.frontiersin.org/articles/10.3389/fncel.2019.00477 [22 Jan. 2023].

581 **Feierstein CE**, **Portugues R**, **Orger MB**. Seeing the whole picture: A comprehensive imaging approach
582 to functional mapping of circuits in behaving zebrafish. *Neuroscience* 296: 26–38, 2015.

583 **Goaillard J-M**, **Marder E**. Ion Channel Degeneracy, Variability, and Covariation in Neuron and Circuit
584 Resilience. *Annual Review of Neuroscience* 44: 335–357, 2021.

585 **Goaillard J-M**, **Taylor AL**, **Pulver SR**, **Marder E**. Slow and Persistent Postinhibitory Rebound Acts as an
586 Intrinsic Short-Term Memory Mechanism. *J Neurosci* 30: 4687–4692, 2010.

587 **Goaillard J-M**, **Taylor AL**, **Schulz DJ**, **Marder E**. Functional consequences of animal-to-animal variation
588 in circuit parameters. *Nature Neuroscience* 12: 1424–1430, 2009.

589 **Golowasch J**, **Bose A**, **Guan Y**, **Salloum D**, **Roeser A**, **Nadim F**. A balance of outward and linear inward
590 ionic currents is required for generation of slow-wave oscillations. *Journal of Neurophysiology* 118:
591 1092–1104, 2017.

592 **Golowasch J**, **Marder E**. Proctolin activates an inward current whose voltage dependence is modified
593 by extracellular Ca^{2+}. *J Neurosci* 12: 810–817, 1992.

594 **Grashow R**, **Brookings T**, **Marder E**. Reliable neuromodulation from circuits with variable underlying
595 structure. *PNAS* 106: 11742–11746, 2009.

596 **Hageter J**, **Waalkes M**, **Starkey J**, **Copeland H**, **Price H**, **Bays L**, **Showman C**, **Laverty S**, **Bergeron SA**,
597 **Horstick EJ**. Environmental and Molecular Modulation of Motor Individuality in Larval Zebrafish [Online].
598 *Frontiers in Behavioral Neuroscience* 15,
599 2021https://www.frontiersin.org/articles/10.3389/fnbeh.2021.777778 [3 May 2023].

600 **Haldane JBS**. The Measurement of Variation. *Evolution* 9: 484–484, 1955.

601 **Hamood AW**, **Haddad SA**, **Otopalik AG**, **Rosenbaum P**, **Marder E**. Quantitative Reevaluation of the
602 Effects of Short- and Long-Term Removal of Descending Modulatory Inputs on the Pyloric Rhythm of the
603 Crab, Cancer borealis. *eNeuro* 2, 2015.

604 **Hamood AW**, **Marder E**. Animal-to-Animal Variability in Neuromodulation and Circuit Function. *Cold*
605 *Spring Harb Symp Quant Biol* 79: 21–28, 2014.

606 **Hamood AW**, **Marder E**. Consequences of acute and long-term removal of neuromodulatory input on
607 the episodic gastric rhythm of the crab Cancer borealis. *Journal of Neurophysiology* 114: 1677–1692,
608 2015.

609 **Harris-Warrick RM**. Neuromodulation and flexibility in Central Pattern Generator networks. *Current*
610 *Opinion in Neurobiology* 21: 685–692, 2011.

611 **Hentschke H**. abfload [Online]. *abfload*
612 2011.https://www.mathworks.com/matlabcentral/fileexchange/6190-abfload [30 Nov. 2020].

613 **Khorkova O**, **Golowasch J**. Neuromodulators, not activity, control coordinated expression of ionic
614 currents. *J Neurosci* 27: 8709–18, 2007.

615 **Li X**, **Bucher D**, **Nadim F**. Distinct Comodulation Rules of Synapses and Voltage-Gated Currents
616 Coordinate Interactions of Multiple Neuromodulators. *J Neurosci* 38: 8549, 2018.

617 **Maloney RT**. Neuromodulation and Individuality [Online]. *Frontiers in Behavioral Neuroscience* 15,
618 2021https://www.frontiersin.org/articles/10.3389/fnbeh.2021.777873 [3 May 2023].

619 **Marder E**. Neuromodulation of Neuronal Circuits: Back to the Future. *Neuron* 76: 1–11, 2012.

620 **Marder E**, **Bucher D**. Understanding Circuit Dynamics Using the Stomatogastric Nervous System of
621 Lobsters and Crabs. *Annual Review of Physiology* 69: 291–316, 2007.

622 **Marder E**, **O'Leary T**, **Shruti S**. Neuromodulation of Circuits with Variable Parameters: Single Neurons
623 and Small Circuits Reveal Principles of State-Dependent and Robust Neuromodulation. *Annual Review of*
624 *Neuroscience* 37: 329–346, 2014.

625 **Marder E**, **Thirumalai V**. Cellular, synaptic and network effects of neuromodulation. *Neural Netw* 15:
626 479–93, 2002.

627 **Marder E**, **Weimann JM**. Modulatory control of multiple task processing in the stomatogastric
628 nervous system. In: *Neurobiology of Motor Programme Selection: New Approaches to Mechanisms of*
629 *Behavioral Chice*, edited by Kien J, McCrohan C, Winlow W. Pergamon, p. 3–19.

630 **Moujaes F**, **Preller KH**, **Ji JL**, **Murray JD**, **Berkovitch L**, **Vollenweider FX**, **Anticevic A**. Toward Mapping
631 Neurobehavioral Heterogeneity of Psychedelic Neurobiology in Humans. *Biological Psychiatry* 0, 2022.

632 **Nadim F**, **Bucher D**. Neuromodulation of neurons and synapses. *Current Opinion in Neurobiology* 29:
633 48–56, 2014.

Nassim C. Good Enough. In: *Lessons from the Lobster: Eve Marder's Work in Neuroscience*.

Nusbaum MP, **Blitz DM**, **Marder E**. Functional consequences of neuropeptide and small-molecule co-transmission. *Nature Reviews Neuroscience* 18: 389–403, 2017.

Palavicino-Maggio CB, **Sengupta S**. The Neuromodulatory Basis of Aggression: Lessons From the Humble Fruit Fly [Online]. *Frontiers in Behavioral Neuroscience* 16, 2022https://www.frontiersin.org/articles/10.3389/fnbeh.2022.836666 [3 May 2023].

Prinz AA, **Bucher D**, **Marder E**. Similar network activity from disparate circuit parameters. *Nat Neurosci* 7: 1345–52, 2004.

Ransdell JL, **Nair SS**, **Schulz DJ**. Neurons within the Same Network Independently Achieve Conserved Output by Differentially Balancing Variable Conductance Magnitudes. *J Neurosci* 33: 9950–9956, 2013.

Rihani K, **Sachse S**. Shedding Light on Inter-Individual Variability of Olfactory Circuits in Drosophila. *Front Behav Neurosci* 16: 835680, 2022.

Russo AF. Overview of Neuropeptides: Awakening the Senses? *Headache* 57 Suppl 2: 37–46, 2017.

Schneider AC, **Fox D**, **Itani O**, **Golowasch J**, **Bucher D**, **Nadim F**. Frequency-Dependent Action of Neuromodulation. *eNeuro* 8: ENEURO.0338-21.2021, 2021.

Schneider AC, **Itani O**, **Bucher D**, **Nadim F**. Neuromodulation reduces interindividual variability of neuronal output. *eNeuro* , 2022. doi:10.1523/ENEURO.0166-22.2022.

Swensen AM, **Marder E**. Multiple Peptides Converge to Activate the Same Voltage-Dependent Current in a Central Pattern-Generating Circuit. *J Neurosci* 20: 6752–6759, 2000.

Swensen AM, **Marder E**. Modulators with Convergent Cellular Actions Elicit Distinct Circuit Outputs. *J Neurosci* 21: 4050–4058, 2001.

Tamvacakis AN, **Lillvis JL**, **Sakurai A**, **Katz PS**. The Consistency of Gastropod Identified Neurons Distinguishes Intra-Individual Plasticity From Inter-Individual Variability in Neural Circuits [Online]. *Frontiers in Behavioral Neuroscience* 16, 2022https://www.frontiersin.org/articles/10.3389/fnbeh.2022.855235 [3 May 2023].

Temporal S, **Desai M**, **Khorkova O**, **Varghese G**, **Dai A**, **Schulz DJ**, **Golowasch J**. Neuromodulation independently determines correlated channel expression and conductance levels in motor neurons of the stomatogastric ganglion. *Journal of Neurophysiology* 107: 718–727, 2011.

Thirumalai V, **Prinz AA**, **Johnson CD**, **Marder E**. Red pigment concentrating hormone strongly enhances the strength of the feedback to the pyloric rhythm oscillator but has little effect on pyloric rhythm period. *J Neurophysiol* 95: 1762–70, 2006.

Tobin A-E, **Cruz-Bermúdez ND**, **Marder E**, **Schulz DJ**. Correlations in Ion Channel mRNA in Rhythmically Active Neurons. *PLOS ONE* 4: e6742, 2009.

667 **Tran T**, **Unal CT**, **Severin D**, **Zaborszky L**, **Rotstein HG**, **Kirkwood A**, **Golowasch J**. Ionic current
668 correlations are ubiquitous across phyla. *Sci Rep* 9: 1687, 2019.

669 **Van Rossum G**, **Drake FL**. *Python 3 Reference Manual*. Scotts Valley, CA: CreateSpace, 2009.

670 **Xu J**, **Lopez AJ**, **Hoque MM**, **Borich MR**, **Kesar TM**. Temporal Profile of Descending Cortical
671 Modulation of Spinal Excitability: Group and Individual-Specific Effects [Online]. *Frontiers in Integrative*
672 *Neuroscience* 15, 2022https://www.frontiersin.org/articles/10.3389/fnint.2021.777741 [3 May 2023].

673

674 # 9 Figure legends

675 **Figure 1: The stomatogastric nervous system (STNS) of crabs.**

676 **(A)** Schematic of the STNS of the crab *C. borealis*. Neurons of the pyloric circuit are located in the
677 stomatogastric ganglion (STG). They receive input from neuromodulatory projection neurons
678 that originate in the paired commissural ganglia (CoG) and the unpaired esophageal ganglion
679 (OG) and send their axons through the stomatogastric nerve (stn). Pyloric motor neurons project
680 their axons through the lateral ventricular (lvn), pyloric dilator (pdn) and pyloric (pyn) nerves. The
681 extracellular recording sites are indicated by circles.

682 **(B)** The core pyloric circuit consists of a group of pacemaker neurons: The anterior burster (AB) and
683 two pyloric dilator neurons (PD). They inhibit their followers, the lateral pyloric (LP) and 3-5
684 pyloric constrictor neurons (PY). Inhibitory synapses are shown as circles, electrical connections
685 are depicted with resistor symbols.

686 **(C)** The pyloric rhythm and rhythm parameters. The activity of the PD neurons from the pacemaker
687 group is recorded from the pdn. Activity of all neurons can be recorded from the lvn, where LP is
688 typically the largest unit, PD is mid-sized, and PY are the smallest units. PY activity is recorded
689 from the pyn. Cycle period is defined as the time from the beginning of one PD burst (PD on) to
690 the next. Cycle frequency (F_{cycle}) is the inverse of cycle period in seconds. Burst start (on) and end
691 (off) for each neuron is calculated by dividing the latency with respect to PD on by the cycle
692 period. In addition, we counted the number of spikes per burst (#spks) and calculated the
693 average spike frequency (F_{spks}) by dividing #spks-1 by burst duration (off-on).

694 **Figure 2: Comodulation at mid concentrations reduces the interindividual variability of cycle**
695 **period.**

696 **(A)** Schematic indication of neuromodulator target neurons (filled circles) in the different
697 neuromodulatory conditions. In the intact condition, each neuron is targeted by an unknown
698 number of neuromodulators. After decentralization (transection of the stomatogastric nerve), all
699 neuromodulation is removed. Proctolin (PROC, P) targets all pyloric neurons, whereas CCAP (C)
700 and RPCH (R) target only AB and LP neurons.

701 **(B)** Overlapping targets of comodulation by PROC, CCAP, and RPCH. Shading indicates how many of
702 the applied neuromodulators target each neuron of the pyloric circuit.

703 **(C)** Extracellular recordings of the pyloric rhythm from one animal under different neuromodulatory
704 conditions (color coded). After decentralization, we applied increasing numbers (P, PC, PCR) and
705 increasing concentrations ([low]: 10^{-9} M, [mid]: 3 x 10^{-8} M) of neuropeptides (arrows), followed
706 by washing out all neuromodulators.
707 **(D)** Cycle frequency and the corresponding CV (standard deviation / mean) under different
708 modulatory conditions. Individual dots represent data from individual experiments, red bars
709 indicate the mean value. N = 15 animals. Asterisks indicate significant differences between
710 groups (Dunn's post-hoc test, $p \leq 0.05$). Total modulator concentration for [low]: 10^{-9} M; [mid]: 3
711 x 10^{-8} M. ANOVA results in Table 2.

712 **Figure 3: Comodulation at mid concentrations reduces the interindividual variability of pyloric**
713 **rhythm parameters on the circuit output level.**
714 **(A)** Burst start (on) and termination (off) and the corresponding circular variance (1-r, see Methods)
715 under different modulatory conditions (color coded). Individual dots represent data from
716 individual experiments, red bars indicate the circular mean. INSET shows a circular plot of a
717 randomly generated phase dataset (N = 10, $\bar{x}$ = 0.35, μ = 0.15). The length of the r-vector
718 indicates the spread of the data. Markers inside the circle indicate 25%, 50%, and 75% of the
719 radius.
720 **(B)** Sum of eigenvalues from the covariance matrix of the phases for each modulatory condition.
721 N = 15 animals. Asterisks indicate significant differences between groups (Dunn's post-hoc test, $p \leq$
722 0.05). Total modulator concentration for [low]: 10^{-9} M; [mid]: 3 x 10^{-8} M. ANOVA results in Table 2.

723 **Figure 4: Comodulation at mid concentrations reduces the interindividual variability of burst**
724 **parameters on the circuit output level.**
725 **(A)** Average number of spikes (#spks) per burst and corresponding CV for each type of neuron at
726 each modulatory condition (color coded).
727 **(B)** Average spike frequency (F_{spks}) within a burst and corresponding CV for each type of neuron at
728 each modulatory condition (color coded).
729 N = 15 animals. Dots represent values from individual experiments, horizontal bars indicate the mean
730 value. Asterisks indicate significant differences between groups (Dunn's post-hoc test, $p \leq 0.05$).
731 Dagger indicates that this group is different from all others, except other groups marked with dagger.
732 Total modulator concentration for [low]: 10^{-9} M; [mid]: 3 x 10^{-8} M. ANOVA results in Table 2.

Figure 5: Comodulation at mid concentrations reduces the interindividual variability of rhythm parameters on the circuit output level in an independent dataset.

(A) Cycle frequency and the corresponding CV under different modulatory conditions.

(B) Burst start (on) and termination (off) and the corresponding circular variance (1-r, see Methods) under different modulatory conditions (color coded).

(C) Sum of eigenvalues from the covariance matrix of the phases for each modulatory condition.

(D) Average number of spikes (#spks) per burst and corresponding CV for each type of neuron at each modulatory condition (color coded).

(E) Average spike frequency (F_{spks}) within a burst and corresponding CV for each type of neuron at each modulatory condition (color coded).

N = 25 animals. Individual dots represent data from individual experiments, red bars indicate the (circular) mean. Asterisks indicate significant differences between groups (Dunn's or Tukey's post-hoc test (see Methods), $p \leq 0.05$). Dagger indicates that this group is different from all others, except other groups marked with dagger. Total modulator concentration for [mid]: 3×10^{-8} M. ANOVA results in Table 3.

Figure 6: Comodulation does not reduce the interindividual variability of excitability metrics on the single cell level.

(A) Voltage changes of one example LP neuron in response to increasing and decreasing current injection.

(B) *f-I* curve of the experiment in (A). The average spike frequency at each current level (dots and error bars indicate mean ± SD) was fitted with a power function (black line). To calculate *f-I* hysteresis between increasing (filled circles) and decreasing (open circles) levels of current injection, we divided the average spiking frequency in increasing by decreasing current levels between 2 and 4 nA (shaded area).

(C) Fit parameters and hysteresis with the corresponding metric of variability (CV, or SD when CV was not applicable) for different modulatory conditions (color coded). Dots represent values from individual experiments, horizontal bars indicate the mean.

N = 19, except PCR N = 11. Asterisks indicate significant differences between groups (Dunn's post-hoc test, $p \leq 0.05$). Total modulator concentration for [mid]: $1\text{-}3 \times 10^{-8}$ M for P and PC, 3×10^{-8} M for PCR. ANOVA results in Table 4.

763 **Figure 7: Comodulation does not add to the reduction of interindividual variability of rebound**
764 **metrics on the single cell level.**
765 **(A)** An example of the rebound experiment in different modulatory conditions (color coded). Top
766 panels show the spike raster plots for all 5 sweeps. Bottom shows the intracellular voltage of one
767 example sweep. t_0 indicates the time point when LP was released from current injection.
768 **(B)** Spike histograms across all sweeps in different modulatory conditions (color coded).
769 **(C)** Sigmoid fits to the cumulative spike histograms. Dots indicate the sigmoid midpoint. Dashed grey
770 line indicates wash.
771 **(D)** Latency and fit parameters with the corresponding metric of variability (CV, or SD when CV was
772 not applicable) for different modulatory conditions (color coded). Dots represent values from
773 individual experiments, horizontal bars indicate the mean.
774 N = 19, except PCR N = 11. Asterisks indicate significant differences between groups (Dunn's or
775 Tukey's post-hoc test (see Methods), $p \leq 0.05$). Total modulator concentration for [mid]: 1-3 x 10^{-8} M
776 for P and PC, 3 x 10^{-8} M for PCR. ANOVA results in Table 5.

777 **Figure 8: Comodulation does not reduce the interindividual variability of rebound from**
778 **periodic inhibition on the single cell level.**
779 **(A)** One example of LP membrane potential in response to periodic hyperpolarization.
780 **(B)** One example periodic rebound experiment in different modulatory conditions (color coded). Top
781 panels show the spike raster plots for all 20 sweeps. Bottom shows the intracellular voltage of all
782 sweeps. t_0 indicates the time point when LP was released from current injection.
783 **(C)** Spike histogram across the last 10 sweeps in different modulatory conditions.
784 **(D)** Sigmoid fits to the cumulative spike histograms. Dots indicate the sigmoid midpoint.
785 **(E)** Latency and fit parameters with the corresponding metric of variability (CV, or SD when CV was
786 not applicable) for different modulatory conditions (color coded). Dots represent values from
787 individual experiments, horizontal bars indicate the mean.
788 N = 19, except PCR N = 11. No significant differences between groups (ANOVA results in Table 6.).
789 Total modulator concentration for [mid]: 1-3 x 10^{-8} M for P and PC, 3 x 10^{-8} M for PCR.

790 **Figure 9: Neuropeptides at high concentration reduce the interindividual variability of pyloric**
791 **rhythm parameters on the circuit output level.**
792 **(A)** Cycle frequency and the corresponding CV under different modulatory conditions (color coded).

(B) Burst start (on) and termination (off) and the corresponding circular variance (1-r, see Methods) under different modulatory conditions (color coded).

(C) Sum of eigenvalues from the covariance matrix of the phases for each modulatory condition.

(D) Number of spikes per burst and corresponding CV for each type of neuron at different high concentration modulatory conditions (color coded).

(E) Average Spike frequency within a burst and corresponding CV for each type of neuron at each modulatory condition (color coded).

Separate datasets for P and PC, N = 10 each. Individual dots represent data from individual experiments, red bars indicate the mean value. Asterisks indicate significant differences between groups (Dunn's or Tukey's post-hoc test (see Methods), $p \leq 0.05$). Dagger indicates that this group is different from all others. The purple empty bars indicate the value of the variability metric at [mid] PCR from Figures 2 to 4. Total modulator concentration for [high]: 10^{-6} M. ANOVA results in Table 7.

Figure 10: Changes in variability of burst attributes and activity phases depend on the regulation of I_{MI} levels across different neurons in a family of model circuits.

(A) Schematic diagram of neurons and ionic currents included in the model.

(B) The modulatory current I_{MI} *I-V* relationship as modeled. Different levels of modulatory input change the maximal conductance g_{MI}, resulting in the changes in the *I-V* relationship as shown (increase shown from grey to black).

(C) Example voltage activity of the four neuron types used in the models at a mid-level modulation of g_{MI} for all neurons shows the triphasic pyloric activity.

(D) Change in the variability (measured as CV) of the circuit output attributes, F_{cycle}, LP #*spks*, LP F_{spks}, PY #*spk*, PY F_{spks} across the 175 model circuits, under different levels of modulatory input. Modulatory input is modeled by increasing g_{MI} from its baseline unmodulated value, from 1x to 1.75x in 13 multiplicative steps, across the whole family of model circuits. g_{MI} was increased independently in each of the three neuron groups (pacemakers AB/PD, LP, PYs), resulting in a 3D grid. For each attribute (row) each panel represents the increase in pacemaker g_{MI} on the horizontal axis and the increase in LP g_{MI} on the vertical axis. The increase in PY g_{MI} is represented in different panels from left to right. Change in CV (with respect to the unmodulated state) is plotted as a heatmap where colors from blue-to-white-black represent decreased-no change-increased CV (see scalebar) of that attribute. Therefore, the left bottom square (white) of the left

823 panel shows the fully unmodulated family of models and the top right square of the right panel
824 shows the fully modulated family.
825 **(E)** Change in the variability (measured as circular variance 1-r) of the burst phases under different
826 levels of modulatory input. Description is as in panel D, but with red replacing blue for reduction
827 in variability.
828 **(F)** Zoom-in to three representative panels of the 3D reduction of variability grid. Data shown are for
829 three attributes: F_{cycle} (top box, corresponding to arrow-highlighted panel in the top row of D), LP
830 F_{spks} (middle box, corresponding to arrow-highlighted panel in the third row of D) and φLP_{off}
831 (bottom box, corresponding to columns indicated by arrows in each panel in the third row of E).
832 In each group, the change in the normalized distribution of that attribute is shown when g_{MI} is
833 changed along the path and direction shown by the arrow in the colored grid panel. This
834 highlights how the density function narrows (representing reduction in variability) by increasing
835 g_{MI}.
836 **(G)** Regions of reduction in variability for all circuit output attributes. Data are represented as in each
837 row of D or E. Each blue dot represents a point in modulatory parameter space where the
838 variability of all attributes in panel D is reduced by at least 2.5%. Each red dot represents the
839 reduction of variability of all phases in panel E. Each pink dot shows the overlap between blue
840 and red, indicating that reduction of variability of all circuit output attributes occurs only
841 sporadically.

Fig. 1

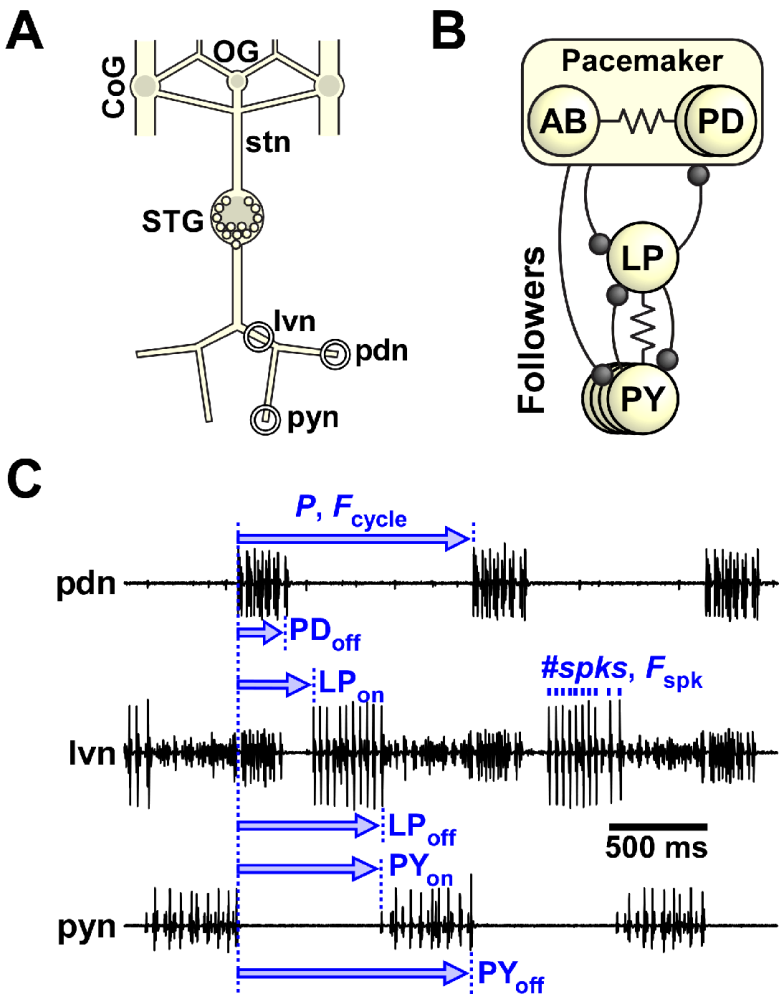
A
CoG
OG
stn
STG
lvn
pdn
pyn
B
Pacemaker
AB
PD
LP
PY
Followers
C
P, F cycle
pdn
PD off
LP on
#spks, F spk
lvn
LP off
500 ms
PY on
pyn
PY off

Fig. 2

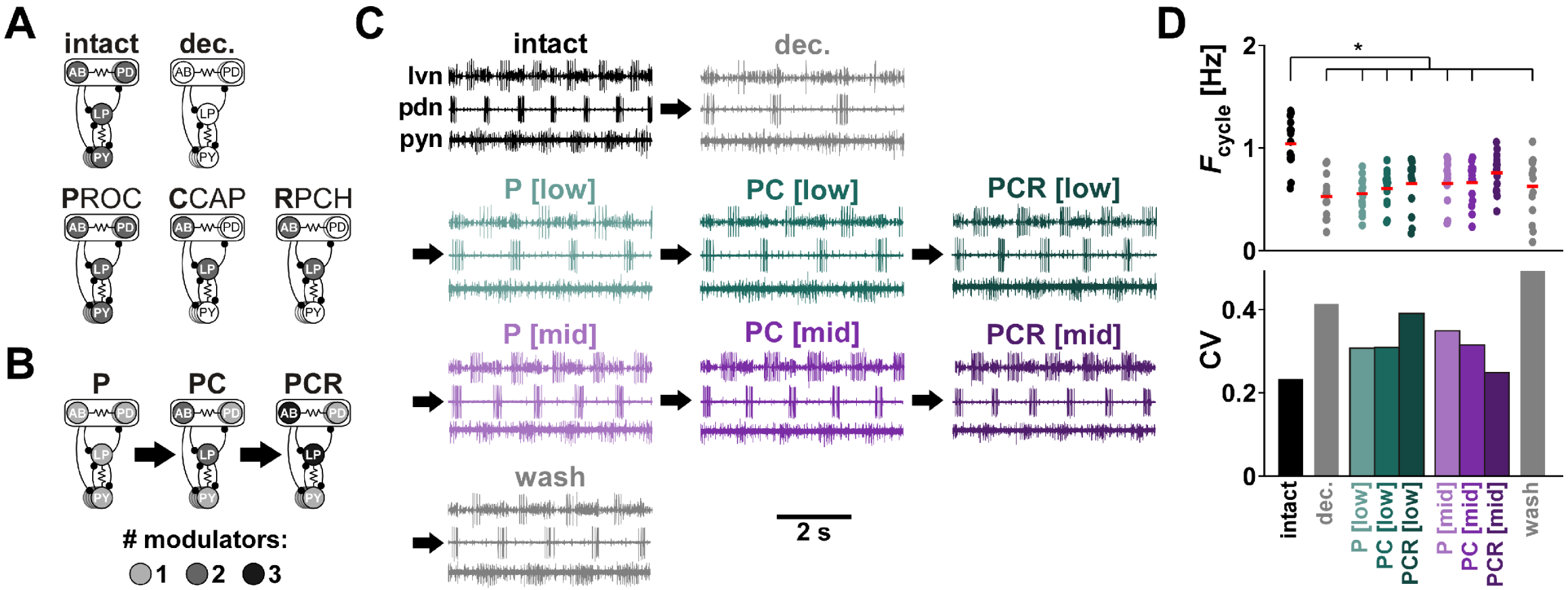
A
intact
dec.
PROC
CCAP
RPCH
B
P
PC
PCR
modulators:
1
2
3
C
intact
dec.
lvn
pdn
pyn
P [low]
PC [low]
PCR [low]
P [mid]
PC [mid]
PCR [mid]
wash
2 s
D
F_{cycle} [Hz]
CV
intact
dec.
P [low]
PC [low]
PCR [low]
P [mid]
PC [mid]
PCR [mid]
wash

Fig. 3

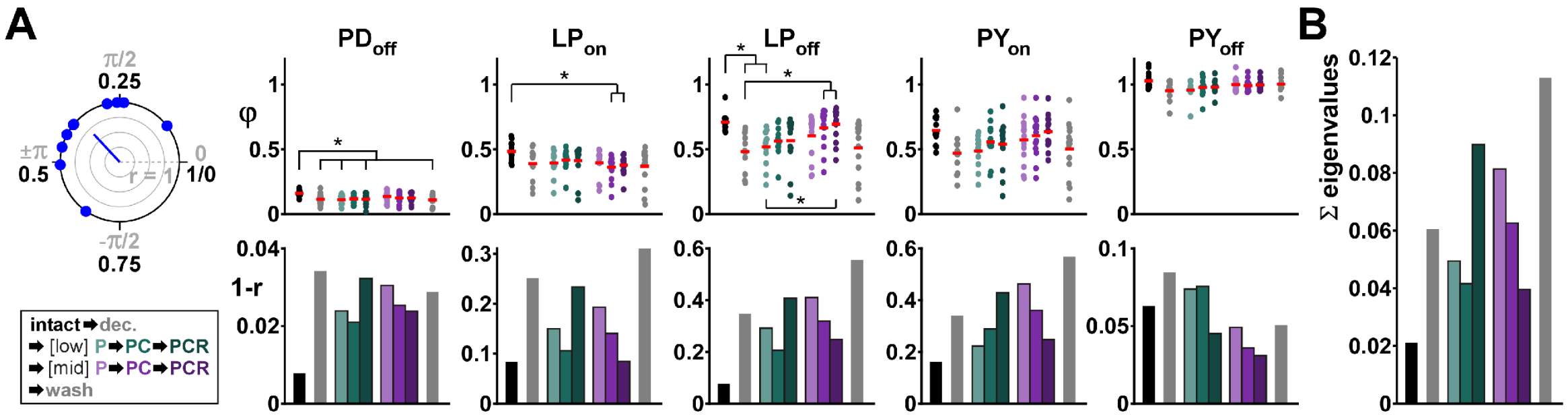
A
π/2
0.25
±π
0.5
0
1/0
r = 1
-π/2
0.75
intact ➡ dec.
➡ [low] P ➡ PC ➡ PCR
➡ [mid] P ➡ PC ➡ PCR
➡ wash
PD off
LP on
LP off
PY on
PY off
φ
1-r
B
Σ eigenvalues

Fig. 4

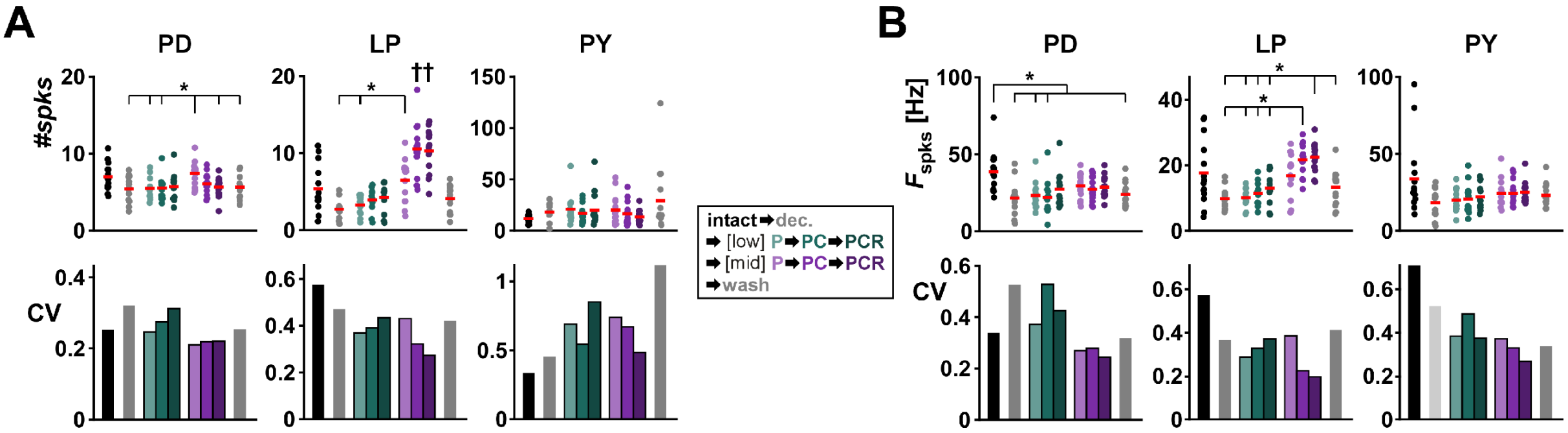
A
PD
LP
PY
#spks
CV
*
††
intact➡dec.
➡ [low] P➡PC➡PCR
➡ [mid] P➡PC➡PCR
➡wash
B
PD
LP
PY
F_{spks} [Hz]
CV

Fig. 5

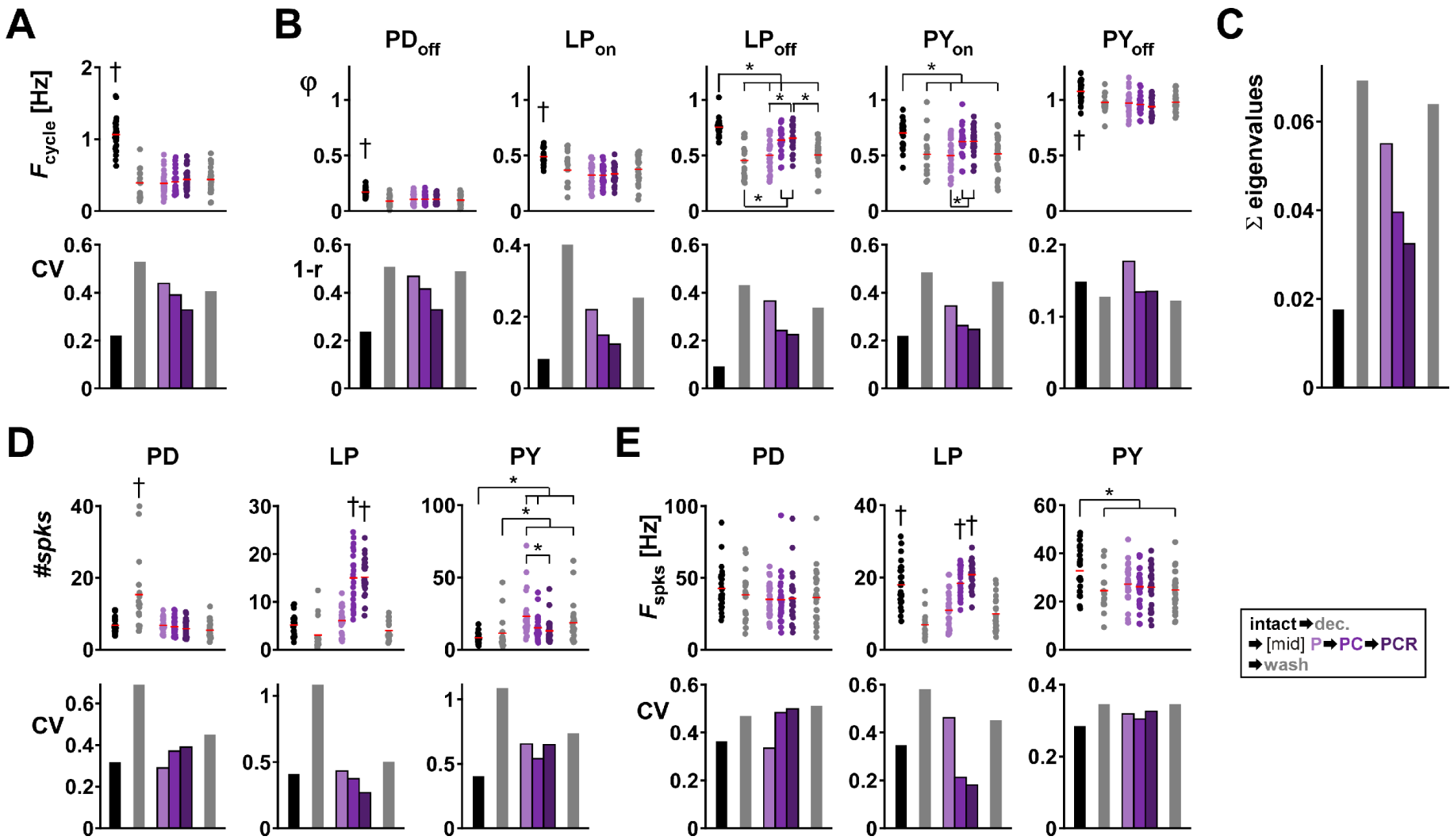
A
B
C
D
E
PD$_{off}$
LP$_{on}$
LP$_{off}$
PY$_{on}$
PY$_{off}$
PD
LP
PY
F_{cycle} [Hz]
CV
φ
1-r
Σ eigenvalues
#spks
F_{spks} [Hz]
intact➡dec.
➡[mid] P➡PC➡PCR
➡wash

Fig. 6

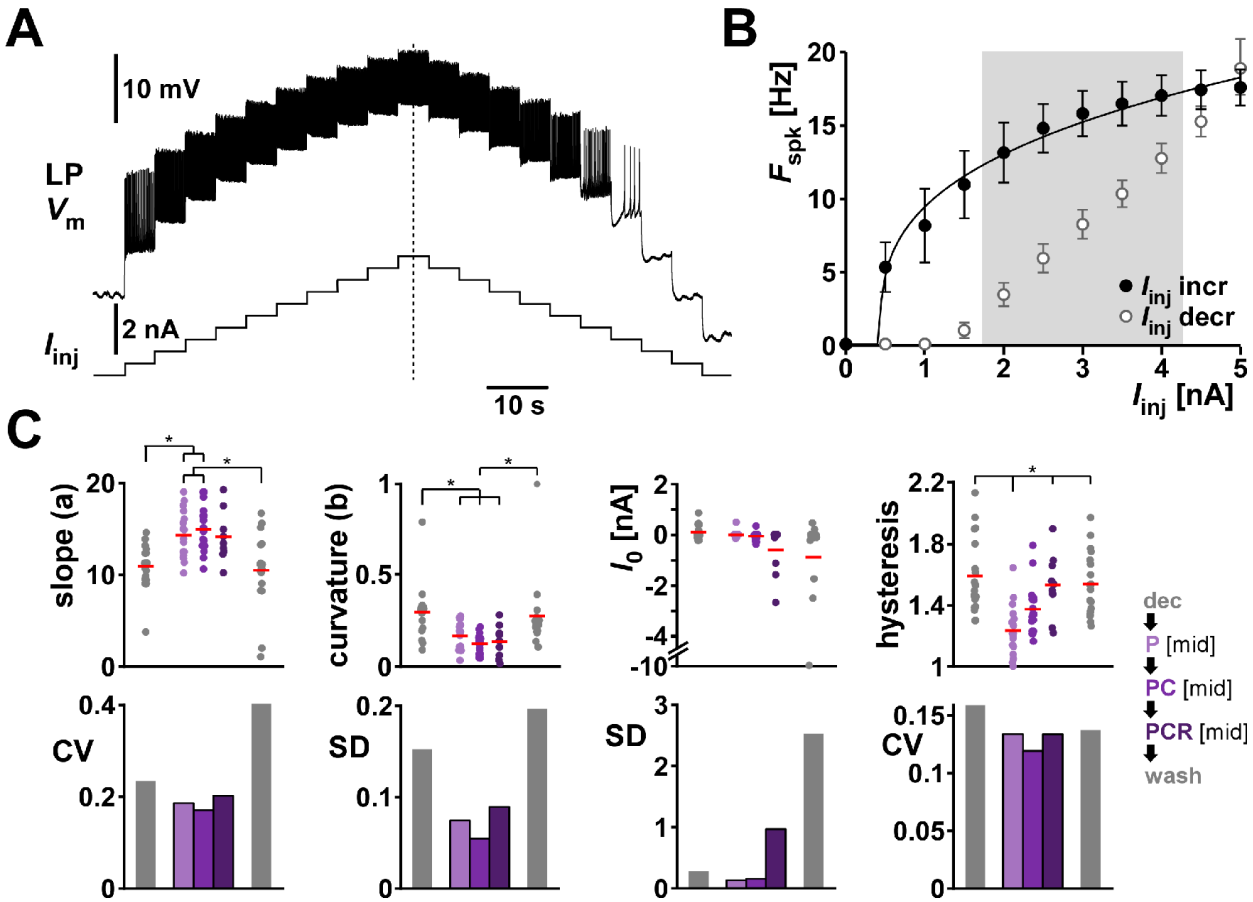
A
10 mV
LP
V_m
2 nA
I_{inj}
10 s
B
F_{spk} [Hz]
I_{inj} incr
I_{inj} decr
I_{inj} [nA]
C
slope (a)
curvature (b)
I_0 [nA]
hysteresis
CV
SD
SD
CV
dec
P [mid]
PC [mid]
PCR [mid]
wash

Fig. 7

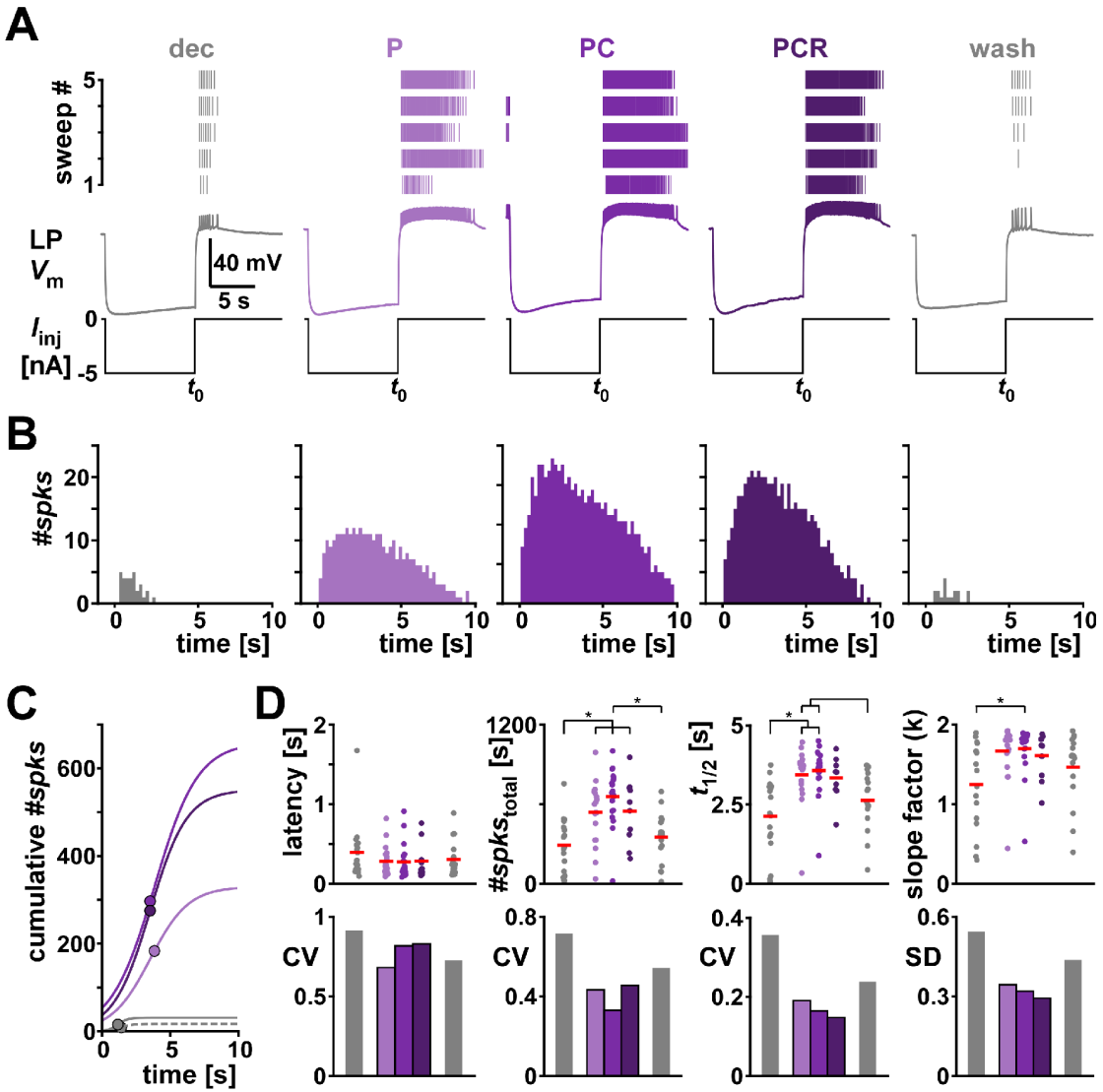

C: dashed line is wash (state in legend)

Fig. 8

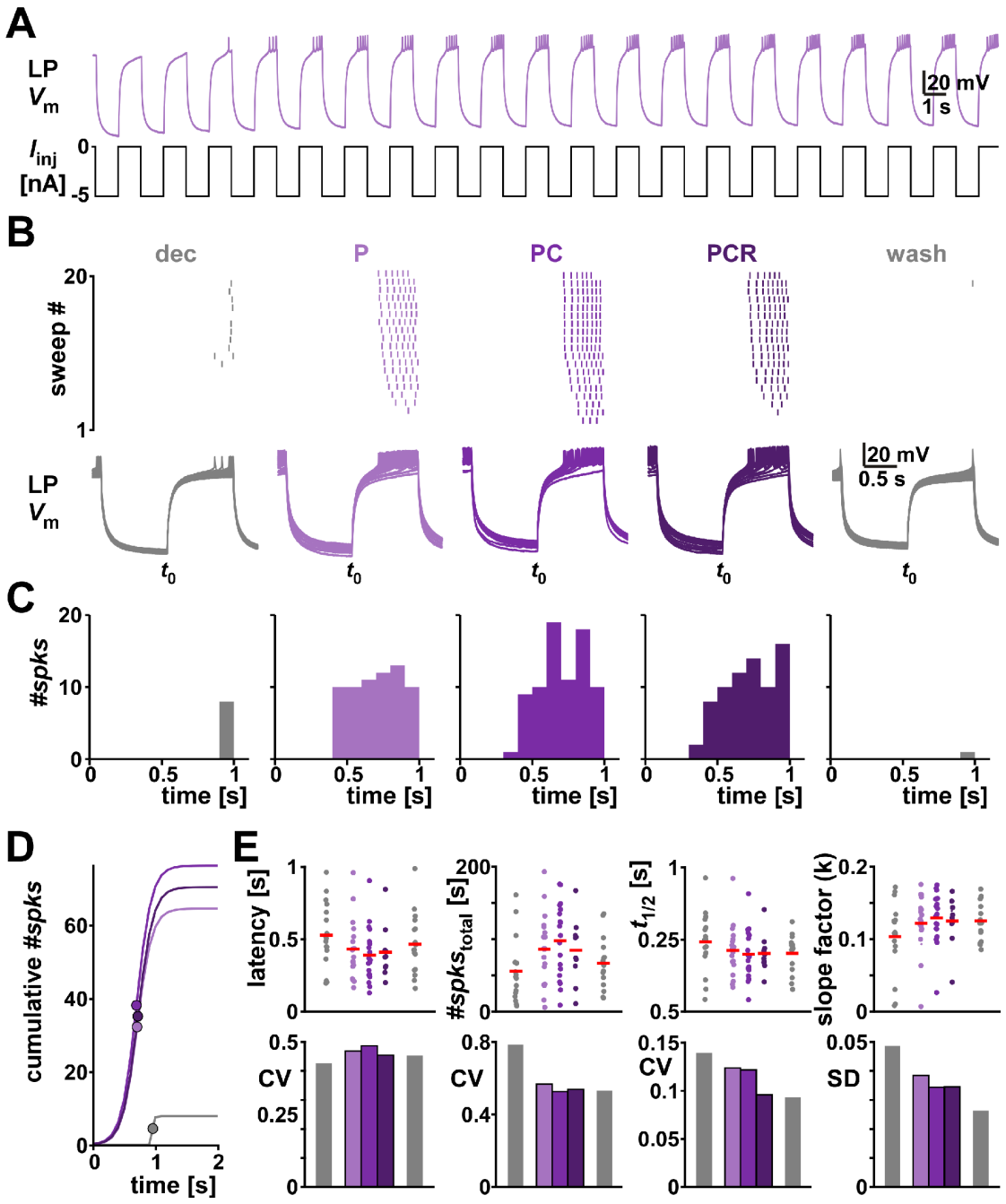
A
LP
V_m
20 mV
1 s
I_{inj}
[nA]
0
-5
B
dec
P
PC
PCR
wash
sweep #
20
1
LP
V_m
20 mV
0.5 s
t_0
C
#spks
20
10
0
0
0.5
1
time [s]
D
cumulative #spks
60
40
20
0
0
1
2
time [s]
E
latency [s]
1
0.5
0
CV
0.5
0.25
0
#spks$_{total}$ [s]
200
0
CV
0.8
0.4
0
$t_{1/2}$ [s]
1
0.25
0.5
CV
0.15
0.1
0.05
0
slope factor (k)
0.2
0.1
0
SD
0.05
0

Fig. 9

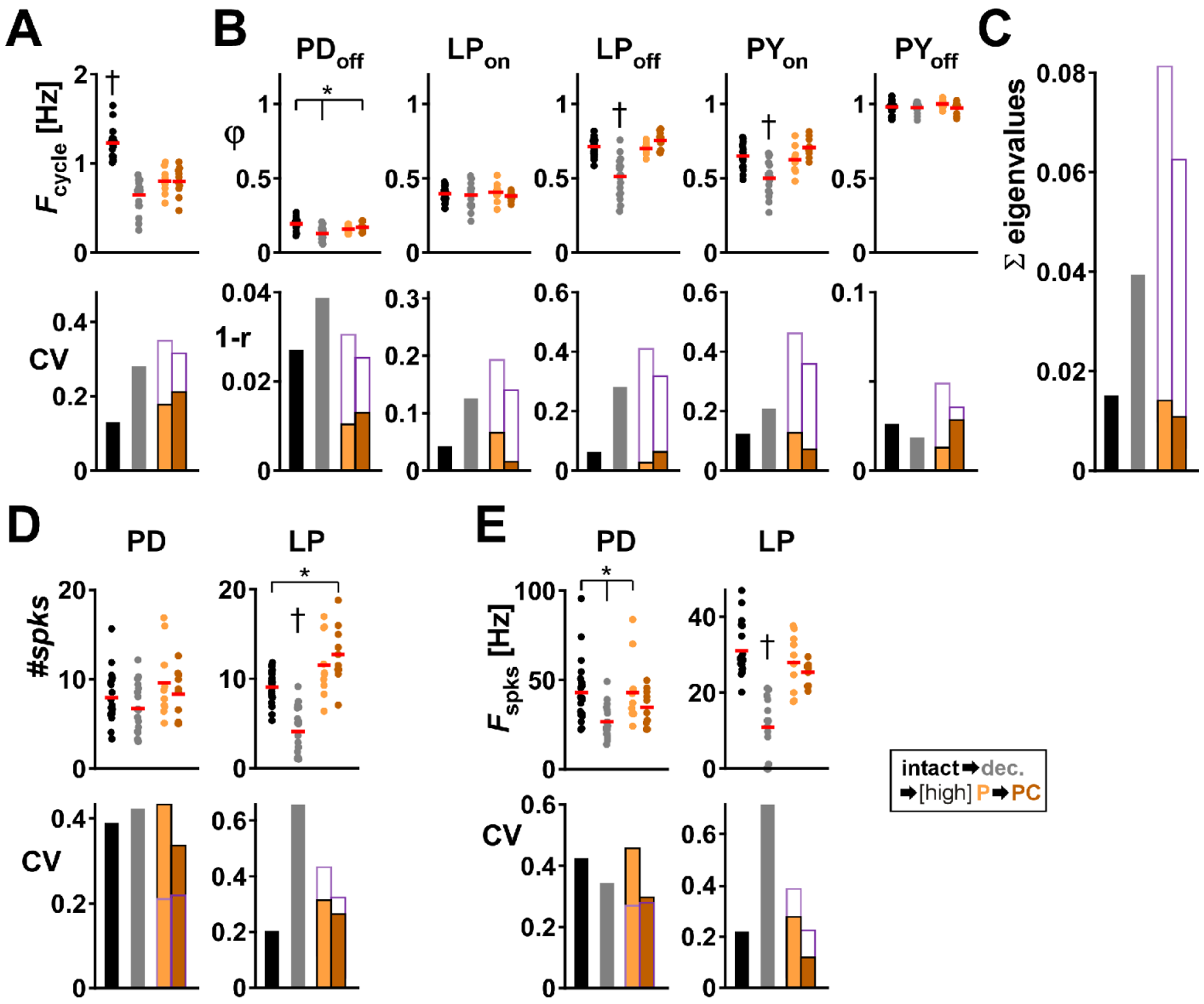
A
B
C
D
E
PD_off
LP_on
LP_off
PY_on
PY_off
F_cycle [Hz]
φ
1-r
CV
Σ eigenvalues
PD
LP
#spks
F_spks [Hz]
intact➡dec.
➡[high] P➡PC

Fig. 10

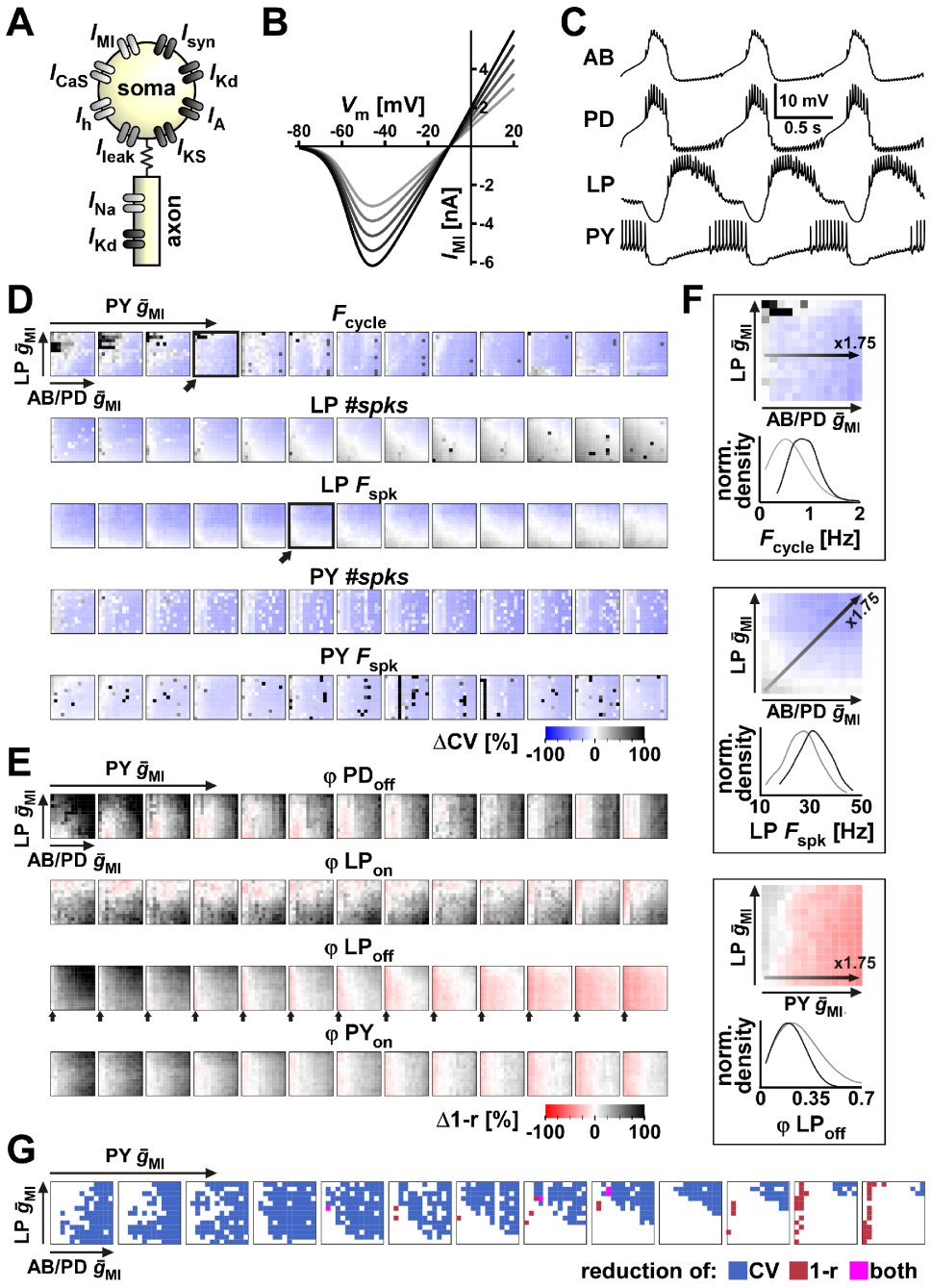
A
soma
axon
B
V_m [mV]
I_{MI} [nA]
C
AB
PD
LP
PY
10 mV
0.5 s
D
PY $\bar{g}_{MI}$
LP $\bar{g}_{MI}$
AB/PD $\bar{g}_{MI}$
F_{cycle}
LP #spks
LP F_{spk}
PY #spks
PY F_{spk}
ΔCV [%]
E
φ PD_{off}
φ LP_{on}
φ LP_{off}
φ PY_{on}
Δ1-r [%]
F
x1.75
norm. density
F_{cycle} [Hz]
LP F_{spk} [Hz]
φ LP_{off}
G
reduction of: CV 1-r both